FULL COVERAGE VANE, BLADE TIP, AND BLADE TRAILING EDGE FILM COOLING FOR GAS TURBINE APPLICATIONS USING THE PRESSURE SENSITIVE PAINT MEASUREMENT TECHNIQUE

A Dissertation

by

IZHAR ULLAH

Submitted to the Graduate and Professional School of
Texas A&M University
in partial fulfillment of the requirements for the degree of

DOCTOR OF PHILOSOPHY

Chair of Committee,	Lesley M. Wright
Co-Chair of Committee,	Je-Chin Han
Committee Members,	Yassin Hassan
	Michael Pate
Head of Department,	Guillermo Aguilar

December 2021

Major Subject: Mechanical Engineering

ABSTRACT

Researchers in the field of gas turbines are always interested in gas turbine vane and blade heat transfer and film cooling performance under realistic engine flow conditions. Complicated flow patterns are present around the three-dimensional airfoils. Therefore, it is necessary to carry out testing on a three-dimensional vane and blade in a wind tunnel that closely simulates the real engine flow. Both annular and linear cascades are used to study the film cooling effectiveness on vane surfaces as well as on the blade tip and trailing edge using the pressure sensitive paint (PSP) measurement technique.

The first study is an experimental study of film cooling effectiveness on two real scale turbine vanes in a 3-vane annular cascade. The cascade is connected to a high flow steady compressor to provide the mainstream flow. The inlet velocity is maintained at 35 m/s at the center line of the annular cascade. Two heavily cooled, real scale turbine vanes are tested with cooling holes on the pressure and suction surfaces. Vane 1 has 645 cooling holes distributed around the vane. Vane 2 has an additional two row of holes at the near leading edge SS of the vane. The MFR is varied from 3.12% to 4.82%. Increasing the MFR increases the film effectiveness. The introduction of additional rows of cooling holes resulted in re-distribution of coolant from the pressure surface to the suction surface.

The second study is an experimental study of film cooling effectiveness on the blade tip in a stationary, linear cascade. The cascade is mounted in a blowdown facility with controlled inlet and exit Mach numbers of 0.29 and 0.75, respectively. The free stream turbulence intensity is measured to be 13.5 % upstream of the blade's leading edge.

A flat tip design is studied, having a tip gap of 1.6%. The blade tip is designed to have 15 shaped film cooling holes along the near-tip pressure side (PS) surface. Fifteen vertical film cooling holes are placed on the tip near the pressure side. The cooling holes are divided into a 2-zone plenum to locally maintain the desired blowing ratios based on the external pressure field. Two coolant ejection scenarios are considered by ejecting coolant through the tip holes only and both tip and PS surface holes together. The blowing ratio (M) and density ratio (DR) effects are studied by testing at blowing ratios of 0.5, 1.0, and 1.5 and three density ratios of 1.0, 1.5, and 2.0. Over-tip flow leakage is also studied by measuring the static pressure distributions on the blade tip using the pressure sensitive paint (PSP) measurement technique. In addition, detailed film cooling effectiveness is acquired to quantify the parametric effect of blowing ratio and density ratio on a plane tip design. A positive blowing ratio and density ratio effect is witnessed. Introduction of coolant injection also reduces the over-tip flow leakage.

The third study measures the film cooling effectiveness along the trailing edge of a turbine blade. The film effectiveness is measured and analyzed using the pressure sensitive paint (PSP) technique. Two different trailing edge designs are investigated including the standard pressure side cutback and the new alternating discharge design (referred to as a wavy trailing edge design). The alternating discharge design is a new design having a wavy like structure between the pressure and suction surfaces of the trailing edge. The new wavy structure helps discharge the coolant from the trailing edge in a manner so it alternates between the pressure and suction surfaces. Testing is carried out in a five-blade, linear, steady state cascade with inlet and exit Mach numbers of 0.20

and 0.30, respectively. The freestream turbulence intensity is measured to be 10.3% upstream of the blade leading edge. Coolant-to-mainstream mass flow ratios (MFR) of 0.30%, 0.50%, 0.75%, 1.0%, 1.25% and coolant-to-mainstream density ratios (DR) of 1 .0, 1.5 and 2 .0 are examined. The total pressure loss coefficients are also acquired to compare the aerodynamic loss between the two trailing edge designs. The pressure loss coefficient is acquired by traversing a group of pitot static probes across the blade span in a plane downstream of the trailing edge, resulting in a pressure map at the exit plane. A positive MFR and density ratio effect is witnessed with negligible difference in the aerodynamic loss.

DEDICATION

This work is dedicated to my whole family including my parents, my wife, my son, and all of my siblings.

ACKNOWLEDGEMENTS

First and foremost, I would like to thank and acknowledge ALLAH (SWT), the creator and nourisher of the whole universe, for His guidance to the right path, countless blessings, and infinite Mercy. I thank ALLAH (SWT) in the way that pleases Him. Indeed, I have and nor ever had any capability and strength except with the will of ALLAH (SWT). Every second of my life is in complete control of ALLAH (SWT). Every single piece of effort, from minor to major work in this thesis, was only possible with the will and help of ALLAH (SWT). I would also like to send my salutations on the beloved Holy Prophet Muhammad (S.W). The lifestyle of Prophet Muhammad (S.W) is indeed complete guidance for the whole of mankind.

I would also like to sincerely thank Dr. Je-Chin Han and Dr. Lesley Wright for their guidance and support throughout my whole journey at Texas A&M University. I faced many difficulties during my studies. From difficulties in research to difficulties in time management, I must say that I would have never been able to cope with these difficulties without the continuous guidance and support from Dr. Han and Dr. Wright. I would also like to thank Dr. Yassin Hassan, and Dr. Michael Pate for being on my advisory committee and for the valuable suggestions during my studies.

Thanks also to my friends and colleagues in Turbine Heat Transfer Laboratory at Texas A&M University. I want to say my special thanks and gratitude to Chao-Cheng Shiau, Sulaiman Alsaleem, Izzet Sahin, and Yasser Alzahrani for making my stay at the

Turbo-lab a never forgotten moment. I also would like to thank Tim Burdett and Anthony Salinas for helping me out with many tasks.

I am also thankful to the respected scholars & ulama of Islam. Far from home, where many distractions are common, it is very easy to be get off the track and forget the real purpose. With the lectures and writings of our respected ulama, I always gained strength and was reminded of the true purpose. They made me realize that my doctoral degree is not something that I have to use for monetary benefit or gain but it is something I can use to serve Islam and the whole mankind.

Lastly, my studies at Texas A&M University were not possible without the endless prayers of my parents, my wife, and all my siblings. I would like to thank and deeply acknowledge my parents, my wife, my son and all my siblings for being there for me always and consistently praying for me. May ALLAH (SWT) keep you all protected and guided.

CONTRIBUTORS AND FUNDING SOURCES

Contributors

This work was supervised by a dissertation committee consisting of Dr. Lesley Wright as the chair, Dr. Je-Chin Han as the co-chair, Dr. Yassin Hassan of the Department of Nuclear Engineering, and Dr. Michael Pate of the Department of Mechanical Engineering as members. In addition, Dr. Rodolfo Vaghetto of the Department of Nuclear Engineering, attended the oral defense (final examination) of this dissertation.

The experiment data taking in section 3 was assisted by Chao-Cheng Shiau. The data taking in section 4 was assisted by Sulaiman Alsaleem. The data taking in section 5 was assisted by Tim Burdett.

All other work for this dissertation was completed by the student, under the advisement of Dr. Lesley Wright of the Department of Mechanical Engineering.

Funding Sources

Graduate study was supported by the Graduate Research Assistantship from Dr. Je-Chin Han through Siemens Energy and Marcus Easterling Endowment Fund. In addition, the study was also supported by Graduate Research Fellowship from the J. Mike Walker ’66 Department of Mechanical Engineering.

NOMENCLATURE

Symbols

A	Area [m^2]; amplitude of wavy structure [mm]
a	Upstream width of land [mm]
AOI	Area of interest
b	Downstream width of land [mm]
C	Vane chord length [m]; concentration by volume [-]
c	Length of cutback slot [mm]
CCD	Charge-coupled device
C_d	Discharge coefficient
d	Cooling hole diameter [m]; upstream height of cutback slot [mm]
DR	Coolant-to-mainstream density ratio $= \rho_c/\rho_m$ [-]
e	Downstream height of cutback slot [mm]
H	Height of blade/vane [m]
h	Tip gap
I	Intensity [-]
L	True suction side surface or pressure side surface length [m]; Blade passage length [m]
l	Hole length [mm]
LE	Leading edge of vane/blade;
LED	Light-emitting device

M	Blowing ratio $= \rho_c v_c / \rho_m v_m$ [-]
$\dot{m}$	Mass flow rate [kg/s]
Ma	Mach number [-]
MFR	Coolant-to-mainstream mass flow ratio $= \dot{m}_c / \dot{m}_m$ [-]
n	Number of the cooling hole in a given row [-]
P	Pressure [Pa]
p	Hole pitch
PS	Pressure surface
s	Slot thickness
SH	Shaped holes
SL	Stagnation lines
SS	Suction surface
t	Lip thickness
TE	Trailing edge
Tu	Turbulence intensity [%]
v	Velocity [m/s]
W	Molecular weight [kg]
w	Thickness of wavy TE [mm]
X/x	Distance from the leading edge of hardware [m]

Greek Symbols

α	Expansion angle of cutback slot [deg]
γ	Specific heat ratio [-]

η	Film cooling effectiveness [-]
ρ	Fluid density [kg/m^3]
λ	Wavelength of wavy TE structure [mm]

Subscripts

air	Property with air injection
aw	Adiabatic wall
ax	Parameter in axial direction
b	Black condition
c	Coolant
fg	Property with foreign gas injection
m	Mainstream
ref	Reference condition
s	Static (for pressure and temperature)
t	Total (for pressure)
w	Impermeable wall

TABLE OF CONTENTS

Page

ABSTRACT ii

DEDICATION v

ACKNOWLEDGEMENTS vi

CONTRIBUTORS AND FUNDING SOURCES viii

NOMENCLATURE ix

TABLE OF CONTENTS xii

LIST OF FIGURES xiv

LIST OF TABLES xvii

1. INTRODUCTION 1

2. OBJECTIVE 3

3. FILM COOLING COMPARISON OF FULL-SCALE TURBINE VANES USING THE PRESSURE SENSITIVE PAINT TECHNIQUE 4

- 3.1 Literature Review 4
- 3.2 Experimental Setup and Method 7
  - 3.2.1 Three-Vane Annular Sector Cascade 7
  - 3.2.2 Film Cooling System 9
  - 3.2.3 Experimental Method – Pressure-Sensitive Paint 12
- 3.3 Test Matrix 15
- 3.4 Experimental Uncertainty 15
- 3.5 Results and Discussion 16
  - 3.5.1 Pressure Distribution 16
  - 3.5.2 Coolant Distribution & Split 18
  - 3.5.3 MFR effect on film effectiveness 23
  - 3.5.4 Radially averaged film effectiveness comparison 25

4. INFLUENCE OF COOLANT DENSITY ON TURBINE BLADE Tip FILM COOLING AT TRANSONIC CASCADE FLOW CONDITIONS USING THE PRESSURE SENSITIVE PAINT TECHNIQUE 28

4.1 Literature Review 28
4.2 Experimental Setup and Method 32
4.2.1 Three Blade Linear Cascade 32
4.2.2 Film Cooling System 35
4.2.3 Experimental Method – Pressure-Sensitive Paint 37
4.3 Test Matrix 37
4.4 Experimental Uncertainty 39
4.5 Results and Discussion 39
4.5.2 PS & Tip Injection (Shared) 42
4.5.3 PS & Tip Injection (Separate) 46
4.5.4 PS & Tip Injection (Separate) – angled view 48
4.5.5 Leakage Flow 49

5. FILM COOLING AND AERODYNAMIC PERFORMANCE OF PRESSURE SIDE CUTBACK AND ALTERNATING DISCHARGE FOR BLADE TRAILING EDGE COOLING 55

5.1 Literature Review 55
5.2 Experimental Setup and Method 59
5.2.1 Five-Blade Linear Cascade 59
5.2.3 Film Cooling System 62
5.3 Test Matrix 64
5.4 Experimental Uncertainty 64
5.5 Results and Discussion 65
5.5.1 Pressure side cutback film effectiveness 65
5.5.2 Open Literature comparison 70
5.5.4 Aerodynamic Loss 76

6. CONCLUSIONS 81

6.1 Full Scale Turbine Vanes Film Cooling Comparison 81
6.2 Influence of Coolant Density on Turbine Blade Tip 82
6.3 Film Cooling and Aerodynamic Loss Measurement of Pressure Side Cutback and Wavy Trailing Edge Design 83

REFERENCES 85

LIST OF FIGURES

Page

Figure 1. Typical turbine blade with external and internal cooling (Reprinted from Han [1]) 2

Figure 2. Test section assembly (Reprinted from Shiau et al. [6]) 8

Figure 3. Location of cooling holes on the vanes. The rows marked in red are only included on vane 2 11

Figure 4. Location and nomenclature of the film cooling rows on the PS, SS (LE view), and SS (SS View) 11

Figure 5. PSP calibration curve at different temperatures (Reprinted from Shiau et al. [6]) 14

Figure 6. PSP calibration at different angles (Reprinted from Shiau et al. [6]) 14

Figure 7. Static Pressure Distribution 18

Figure 8. Film effectiveness contours and spanwise averages for vane 1(a) and vane 2 (b) 19

Figure 9. Comparison of radially averaged film cooling effectiveness for both vanes at all coolant flow rates 26

Figure 10. Area averaged film effectiveness 27

Figure 11. Turbine blade tip test facility 33

Figure 12. (a) Flow periodicity chart (Reprinted from Narzary et al. [26]) (b) Blade loading curves 34

Figure 13. (a) Blade tip design (b) Blade core (c) Blade tip top cross-sectional view 36

Figure 14. Geometry of film cooling holes 36

Figure 15. Film cooling effectiveness distributions (top view) for tip only injection at all density ratios 41

Figure 16. Laterally averaged film cooling effectiveness for tip only injection at all density ratios 41

Figure 17. Area averaged effectiveness for tip only injection 42

Figure 18. Film cooling effectiveness distributions (top view) for PS & tip (shared) injection at all density ratios 44

Figure 19. Laterally averaged film cooling effectiveness for tip only vs PS & tip (shared) injection 45

Figure 20. Area averaged effectiveness for tip only vs PS & tip (shared) injection 46

Figure 21. Film cooling effectiveness distributions (top view) for PS & tip (separate) injection at all density ratios 47

Figure 22. Laterally averaged film effectiveness for PS & tip (separate) injection for all densities 47

Figure 23. Area averaged effectiveness for PS & tip (separate) injection 48

Figure 24. Film cooling effectiveness distributions (angled view) for PS & tip (separate) injection 49

Figure 25. Static pressure distribution on blade tip with no coolant 52

Figure 26. Static pressure distribution (top view) for all injection scenarios at DR=1.0 53

Figure 27. Laterally averaged static pressure distribution on the PS rim of the tip at DR=1.0 53

Figure 28. Five blade linear cascade (Reprinted from Chen et al. [63]) 60

Figure 29. Loading curve for test blade (Reprinted from Gao et al. [64]) 61

Figure 30. (a) PS Cutback Design view from pressure side, (b) (c) definitions and dimensions 63

Figure 31. (a) Wavy Design view from pressure side, (b) (c) definitions and dimensions of the wavy structure 63

Figure 32. Conceptual view of PS cutback mainstream and coolant interaction 68

Figure 33. Film effectiveness contours for PS cutback showing slots and lands (arrows in red and blue shows mainstream and coolant direction, respectively) 69

Figure 34. Film effectiveness contours for PS cutback sidewalls (arrows in red and blue shows mainstream and coolant direction, respectively) 69

Figure 35. Spanwise averaged effectiveness and area averaged effectiveness for slot, land, sidewalls, and combined 70

Figure 36. Open literature comparison at DR=1.0 71

Figure 37. Conceptual view of wavy TE design mainstream and coolant interaction 74

Figure 38. Film effectiveness contours for wavy tailing edge design (arrows in red and blue shows mainstream and coolant direction, respectively) 74

Figure 39. Spanwise averaged film effectiveness for wavy TE 75

Figure 40. Spanwise averaged film effectiveness for wavy TE vs PS cutback 75

Figure 41. Area averaged film effectiveness comparison for wavy and PS cutback 75

Figure 42. Location of plane for aerodynamic loss measurments 78

Figure 43. Pitot-static probe locations on the downstream measurement plane 78

Figure 44. Aerodynamic loss measurement at x/ C_{ax} = 0.25 for wavy and PS cutback ... 79

Figure 45. Aerodynamic loss measurement at x/ C_{ax} = 0.50 for PS cutback 79

Figure 46. Conceptual view of formation of wake at blade TE 80

Figure 47. Comparison of laterally averaged pressure ratio for both trailing edge configurations 80

LIST OF TABLES

Page

Table 1: Summary of test conditions for two vanes 15

Table 2: Cooling hole locations and coolant flow rates and blowing ratios at different rows for MFR=3.82% 23

Table 3: Summary of test conditions for blade tip testing 38

Table 4: Momentum flux ratios 39

Table 5: Leakage flow as a percentage of mainstream passage flow for all injection cases 54

Table 6: Mainstream flow conditions for testing 61

Table 7: Summary of test conditions for two TE designs 64

1. INTRODUCTION

Gas turbine engines are vital to the aviation and power generation industries. The thermal efficiency of a gas turbine engine is dictated by the turbine inlet temperature. The higher the temperature, the higher is the efficiency of the engine. However, this high inlet temperature is well above the melting temperature of the internal hardware of the engine. Thermal barrier coating (TBC) is one common method used to prevent the hardware from melting; however, the thermal barrier coating comes with very high cost and needs regular replacement and refurbishment. Therefore, in addition to the TBC, different schemes are introduced to effectively cool the turbine components. These schemes are most commonly based on external and internal cooling which are achieved by extracting low temperature air from the compressor flow prior to combustion. The extracted mainstream air is used to cool the turbine component.

The most common external cooling is done by injecting relatively low temperature air through rows of holes in the turbine hardware. This is called film cooling. This low temperature air forms a barrier on the outer surface of the hardware; thus, protecting the desired component from high heat load. Film cooling design is based on the external flow field of the hot gases. It is imperative to have the knowledge of the external flow field to design an efficient and cost-effective cooling scheme. The turbine vanes and blades are exposed to complicated flow fields including, but not limited to, horseshoe vortices, channel vortices, and over-tip flow leakage [1]. A typical turbine blade design with different cooling holes on the endwall, blade surface, blade tip, and trailing edge is shown

in Fig. 1. Therefore, many studies are present in the open literature aimed at improving the cooling arrangements for different turbine components. It is an endless goal of gas turbine designers to continuously improve the engine performance with the introduction of new cooling schemes.

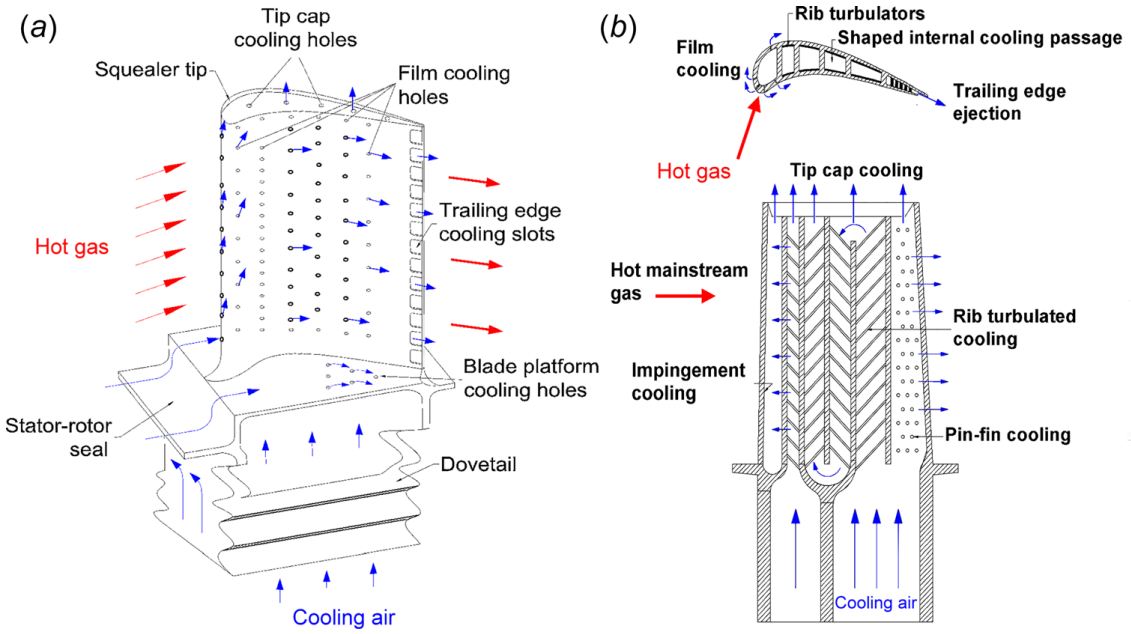

Figure 1. Typical turbine blade with external and internal cooling (Reprinted from Han [1])

2. OBJECTIVE

With knowledge of the importance of the flow field and inlet conditions at the turbine, it is necessary to complete testing under realistic engine flow conditions. Turbine vanes, for example, have a specific flow field due to the flow exiting the combustor followed by the sudden mixing and entrance into the vane passage. This entrance of flow to the turbine vane under extreme turbulence and mixing conditions takes place in a complete annular turbine rig. The annular rig generates channel vortices and horseshoe vortices within the flow. This creates a very high heat load on the turbine vane, and an improper cooling design can lead to hardware failure. Similarly, for the turbine blade, the over-tip flow field is another important factor that dictates the heat transfer on the tip surface. In actual engines, the over-tip flow field is caused by a large pressure difference between the pressure and suction surfaces. Similar engine representative conditions are needed to study the trailing edge of the turbine blade. Since the trailing edge consumes a significant amount of coolant, mixing of the coolant with the mainstream air can have a significant impact on the engine efficiency. It is the objective of this work to study turbine vane, blade tip and blade trailing edge film cooling under engine representative flow conditions to help the gas turbine designer better understand different requirements for designing a better film cooling system.

3. FILM COOLING COMPARISON OF FULL-SCALE TURBINE VANES USING THE PRESSURE SENSITIVE PAINT TECHNIQUE

3.1 Literature Review

Gas turbine vanes experience high temperatures due to the hot gases at the exit of combustion chamber [1]. Therefore, aggressive cooling is required for prolonged operation at higher temperatures. This is achieved by incorporating a proper cooling scheme over the entire vane surface. In order to have appropriate cooling schemes for turbine vanes, knowledge of the flow field around the vane as well as the inlet flow conditions is necessary. For instance, Giller and Schiffer [2] showed the inlet swirl has a great impact on the flow field as well as the film cooling performance of the vane. Qureshi et al. [3] also studied effect of inlet swirl on the vane flow field. Very recently, Lerch et al. [4] studied a fully cooled vane in a high-speed linear cascade under non-uniform combustor flow conditions. They concluded that the shifting of the vane stagnation line has an impact on the film cooling effectiveness of the vane. Similarly, Anthony et al. [5] studied a fully cooled inlet turbine vane in a complete annular sector test section. They studied the film cooling and heat transfer on the pressure surface of the vane and concluded that the cooling performance of the vane is affected by backflow margin and unsteady hot gas ingestion. Shiau et al. [6] studied a complete turbine vane in an annular sector under real engine flow conditions. They studied the endwall film cooling effectiveness and concluded that the endwall film hole distribution in combination with the inlet flow

conditions can change the local flow field near the vane surface, thereby affecting the film cooling effectiveness of the vane.

Studies on a single row of holes shows that the blowing ratio generally has a positive impact on film cooling effectiveness [7-10]. However, since a gas turbine vane is designed to have multiple rows of holes on the pressure (PS), suction (SS), and leading edge (LE) surfaces, it is imperative to study the parametric effect of coolant-to-mainstream mass flow ratio (MFR) or blowing ratio (M) on a fully cooled turbine vane. Gao et al. [11] studied a turbine blade with multiple rows of holes. They concluded that the leading edge holes help to increase film effectiveness on the pressure and suction surfaces. They also witnessed that the suction surface has reduced film effectiveness near the endwall region due to the passage vortex, a typical behavior of coolant on the suction surface. Similarly, Mhetras et al. [12] concluded that the blowing ratio has a positive impact on blade film effectiveness. They also concluded that better SS coverage can be obtained with a smaller number of rows as compared to the PS surface. Narzary et al. [13] also studied a fully cooled turbine blade in a 5-blade linear cascade with uncontrolled coolant flowing to both the PS and SS surfaces. A significant increase in effectiveness was observed with increased blowing ratio for the pressure surface while a moderate increase in effectiveness was observed for the suction surface. Dyson et al. [14] studied a fully cooled turbine vane with 13 rows of holes using an IR technique. Results suggested that the showerhead film cooling effectiveness increases with increasing coolant flow rate while the PS and SS film effectiveness had a moderate increase in effectiveness with an increase in coolant flow rate. Wu et al. [15] studied a turbine vane with 15 rows of cooling holes in a linear cascade

at low speed. The effect of mainstream Reynolds number and coolant flow rate was observed. It was concluded that the MFR has a positive impact on the PS while the SS has a negative impact at higher MFR due to coolant lift-off. They also observed that the coolant on the suction surface converges due to the passage vortices at both the ends of the suction surface. Yao et al. [16] recently studied a fully cooled turbine vane at different MFR conditions. The MFR was reported to have a positive impact on the PS and a negative impact after a certain point on the SS. The leading edge was reported to have the lowest effectiveness due to high external static pressure on the LE surface.

In addition to single vane testing, other studies also compare two identical shaped vanes or blades with different film cooling designs. Zhang et al. [17] tested two blade designs in a single blade linear cascade. The baseline design incorporated cylindrical holes on the pressure and suction surfaces while the improved design had fan shaped holes. A clear positive trend for MFR was witnessed and the new design recorded better film effectiveness as compared to the baseline design. Similar to Zhang et al. [17], Liu et al. [18] carried out testing in a 5-blade linear cascade. Two identical blades, one with cylindrical holes and one with fan shaped holes, were tested. A clear improvement in the new design with fan shaped was seen in terms of film cooling effectiveness.

Most of the previous studies in the open literature are related to the film effectiveness with the coolant flow controlled separately to the pressure and suction surfaces. However, few studies are present in the open literature that consider a complete vane with simultaneous cooling of the pressure and suction surfaces. This study experimentally examines and compares the film cooling effectiveness of two identical

heavily cooled, real scale, turbine vanes with different numbers of film cooling holes under realistic engine inlet flow conditions. The conduction free PSP technique is used to obtain high-fidelity film cooling effectiveness distributions. The parametric effect of varying the coolant-to-mainstream mass flow ratio (MFR) on the local flow behavior and the cooling performance is studied and compared in the form of effectiveness contours and spanwise/area averaged film effectiveness. Results from the current work will provide the engine designers with more insight on designing a cost-effective real scale turbine vane with an effective cooling scheme.

3.2 Experimental Setup and Method

3.2.1 Three-Vane Annular Sector Cascade

Figure 2(a) shows the full scale, three vane annular cascade (green color). These vanes were assembled using the assembly clearances to realize the actual flow field (radial pressure gradient and secondary flows) under real engine flow conditions. The test section is shown in Fig. 2(b). A 450 hp centrifugal compressor is used to provide a volume flow rate of 6.14 m^3/s of mainstream air at the design conditions. The inlet and exit Mach numbers for the cascade is maintained at 0.10 and 0.24, respectively. The Reynolds number is calculated to 350,000 based on the inlet Mach number and chord length (17.5 cm). To simulate the real engine inlet flow conditions (pressure gradient, velocity, and turbulence) due to the combustors and transition pieces, the inlet duct of the test section is transitioned to an annular shaped duct to match the interface of the three vanes. Similarly, a turbulence grid is installed after the transition duct to create approximately 12% turbulence intensity. Details on the turbulence grid can be found in study by Shiau et al.

[6]. The upstream and downstream of the test section has 1.27 cm thick plexiglass windows for optical access. Inlet and exit velocities are measured using pitot static probes at 5.08 cm and 2.45 cm upstream and downstream of the center vane.

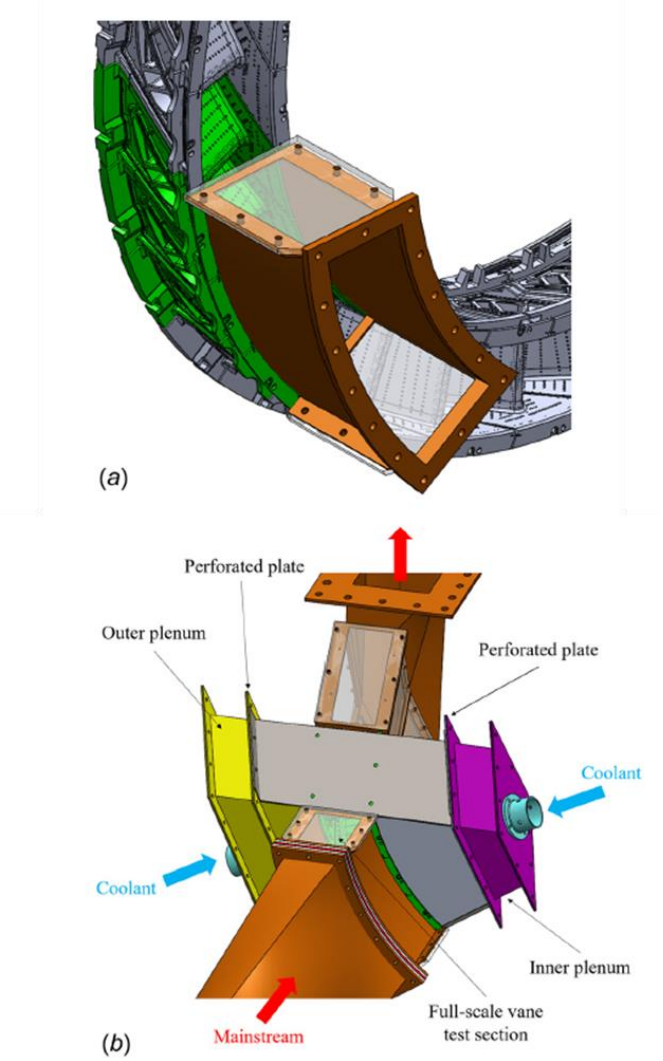

Figure 2. Test section assembly (Reprinted from Shiau et al. [6])

3.2.2 Film Cooling System

Many previous studies have used scaled up or scaled down turbine vanes with coolant supplied separately to the PS and SS. Studies related to a real turbine vane with coolant supplied to both the PS and SS are very rare in open literature. This study considers a turbine vane with the PS and SS open to coolant simultaneously. The film cooling system consists of the coolant source, coolant plenums, and an actual test vane. Coolant (air and foreign gas) is provided from the source (cylinders in case of foreign gas and compressor in case of air) through an orifice meter. After the orifice flow meter, the coolant is divided into the inner and the outer plenum (as shown in Fig. 2(b)). The inner and outer plenums are an annular design, thereby, supplying coolant to the vane through the inner sector and outer sector of the vane. To have uniform distribution of the coolant, a flow deflector and perforated plates are used inside both the plenums (see Shiau et al. [6] for details). Uniformity of the pressures inside the plenum is checked by using two pressure taps each at the inner and outer plenums.

Figure 3 shows the cross-sectional view of the test vanes. The details of the distribution and nomenclature for the cooling holes is also given in Fig 3. Vane 1 is designed with 645 cooling holes (cylindrical and fan shaped) on the vane surface. Six rows at the leading edge (SH1-SH6) are the showerhead cylindrical holes. The pressure surface has six rows of fan shaped holes (P1-P6). Similarly, the suction surface has five rows of fan shaped holes (S1 – S5). One cylindrical hole is also present at both ends (inner ring and outer ring) of each fan shaped row. Vane 2 is similar to vane 1 with an additional two rows of cooling holes on the suction surface as shown in red in Fig.3. These two new rows

account for 71 additional cooling holes as compared to vane 1, making it a total of 716 cooling holes.

Figure 4 shows the vane from different views. From left to right are the vane pressure side (PS), suction side (SS) leading edge, and the suction side (SS) views. These views are also used to capture data which will be presented in the later sections. The showerhead holes (SH1-SH6) and pressure side rows (P1-P6) can be seen in the PS view of Fig. 4. The suction surface view is divided, with S1-S2 shown on the SS (LE view), and S3-S5 shown on the SS view. Two new rows S1-S2 are shown in red in the SS (LE view) for the vane 2 design. The location (x/L) for each row is also shown in Fig. 4.

Since the test vanes have uncontrolled coolant flowing to the PS and SS surfaces, it is important to estimate the coolant distribution on the vane surfaces. The coolant distribution is dictated by different cavities as shown in Fig. 3. The coolant from the inner and the outer plenum is distributed into the vane through three cavities. For vane 1, cavity 1 provides coolant to the leading edge showerhead holes (SH1-SH6) and two rows of shaped holes (P1 and P2) on the pressure side. Cavity 1 also provides coolant to the four rows of holes (S1 -S4) on the suction surface. Cavity 2 provides coolant to two rows of holes (P3 and P4) on the pressure side and one row of holes (S5) on the suction surface. Cavity 3 provides coolant to two rows of holes (P5 and P6) on the pressure surface and the trailing edge. In the case of vane 2, cavity 1 also provides coolant to the additional two rows (marked red in Fig. 3).

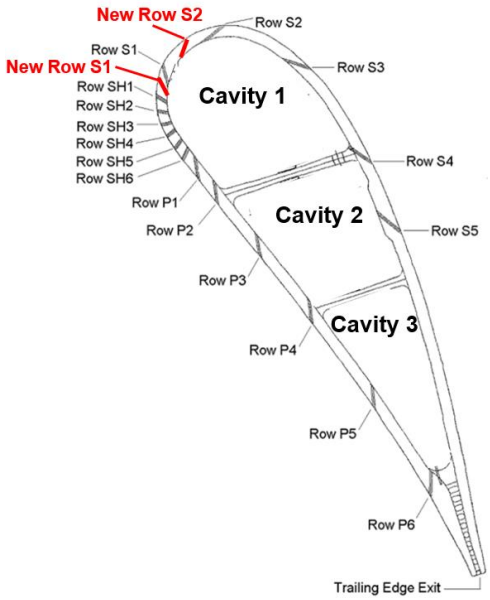

Figure 3. Location of cooling holes on the vanes. The rows marked in red are only included on vane 2

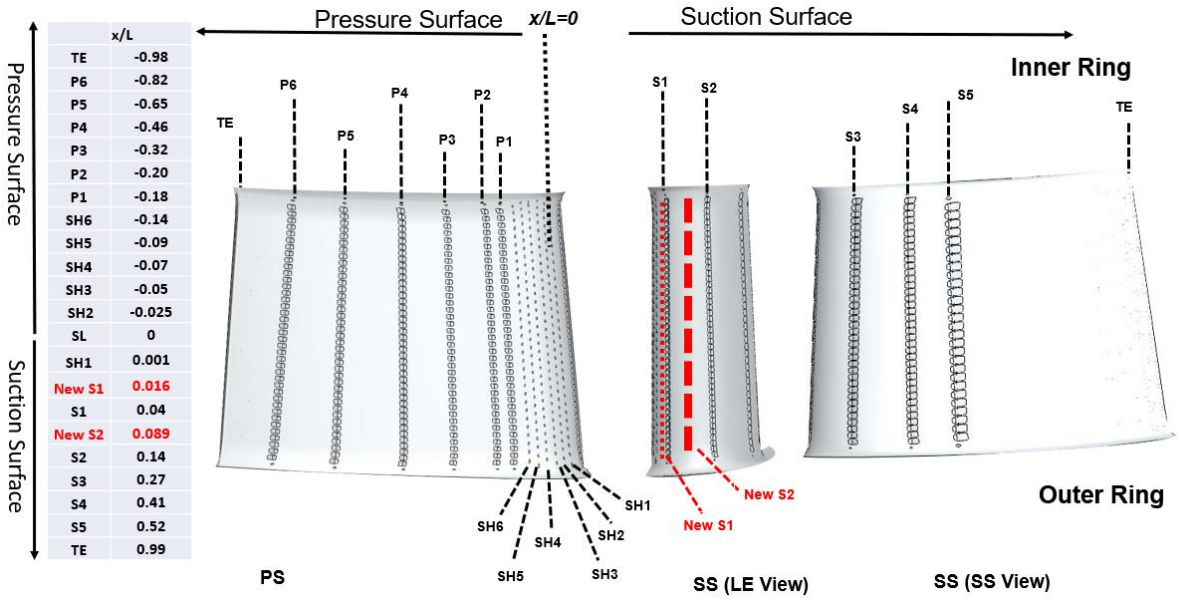

Figure 4. Location and nomenclature of the film cooling rows on the PS, SS (LE view), and SS (SS View)

3.2.3 Experimental Method – Pressure-Sensitive Paint

To quantify the film cooling effectiveness on the vane surface, pressure sensitive paint (PSP) is used. The PSP is applied to the vane surface. The paint is excited using a 400 nm LED light. As soon as the paint is excited with the LED light, it emits radiation of a different wavelength which can be easily captured by a CCD camera. The radiation emitted by the paint is heavily dependent on the oxygen partial pressure (or concentration) on the paint surface. This phenomenon is known as oxygen quenching effect. This relationship between the oxygen partial pressure and the emitted intensity is achieved by a calibration curve. The calibration is carried out in a small box. A test piece with 4 layers of PSP is placed inside the box. Since the current test section has different variables that come into play (for example temperature difference caused by mainstream flow, view angle difference caused by camera location for different views), the calibration is carried out at different temperatures (see Fig. 5) and different view angles (see Fig. 6). The pressure inside the calibration box is varied using a pump and the temperature of the test piece is varied using a heater.

The vane pressure and suction surfaces are first sprayed with black paint to eliminate stray reflection and then sprayed with 4-5 layers of PSP paint. Extreme care is taken while painting the surface since there are hundreds of small film holes. Before spraying with the PSP, the cooling holes are plugged in order to eliminate any blockage of the holes with the paint. After the paint is sprayed, blockages are removed. As a safety precaution, each hole was checked with a thin wire to ensure none of the holes are clogged with paint.

The film cooling effectiveness can be calculated by taking four sets of images. The black image set (I_{blk}) is taken to eliminate background noise. The reference image set (I_{ref}) is taken under no flow conditions with the LED on to provide the reference condition. The air injection image (I_{air}) and foreign gas injection image (I_{fg}) sets are taken with mainstream and coolant on to provide the actual flow conditions. The corresponding oxygen partial pressures on the vane surface are $P_{O_2,air}$ and $P_{O_2,fg}$.

The adiabatic film cooling effectiveness can be expressed as shown in Eq. (1) by using the analogy of heat and mass transfer,

$$\eta = \frac{T_w - T_m}{T_c - T_m} \approx \frac{C_w - C_m}{C_c - C_m} = \frac{C_{O_{2,fg}} - C_{O_{2,air}}}{C_{O_{2,c}} - C_{O_{2,air}}} = 1 - \frac{C_{O_{2,fg}}}{C_{O_{2,air}}} \tag{1}$$

All the concentration terms can be replaced with their corresponding partial pressure terms; Eq. (2) can then be re-written as [19],

$$\eta = 1 - \frac{1}{\left[\left(\frac{P_{O_2,air}/P_{O_2,ref}}{P_{O_2,fg}/P_{O_2,ref}} - 1\right)\frac{W_{fg}}{W_{air}} + 1\right]} \tag{2}$$

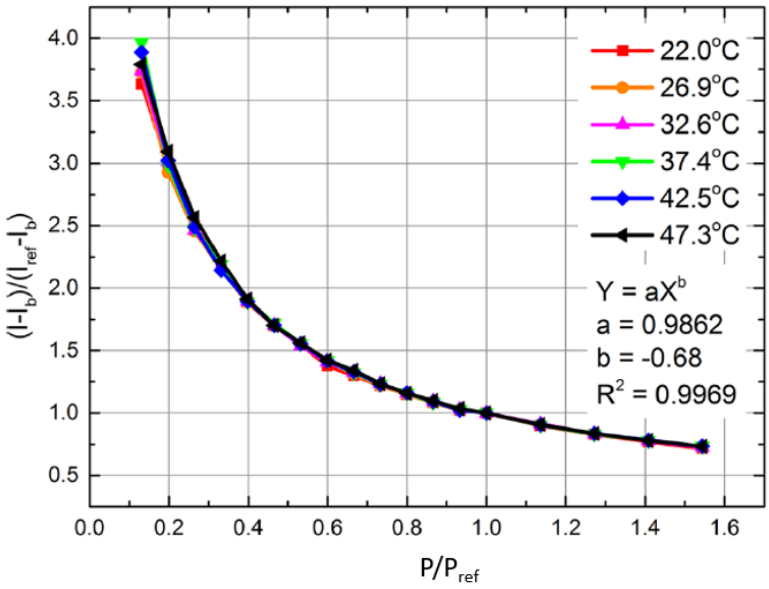

Figure 5. PSP calibration curve at different temperatures (Reprinted from Shiau et al. [6])

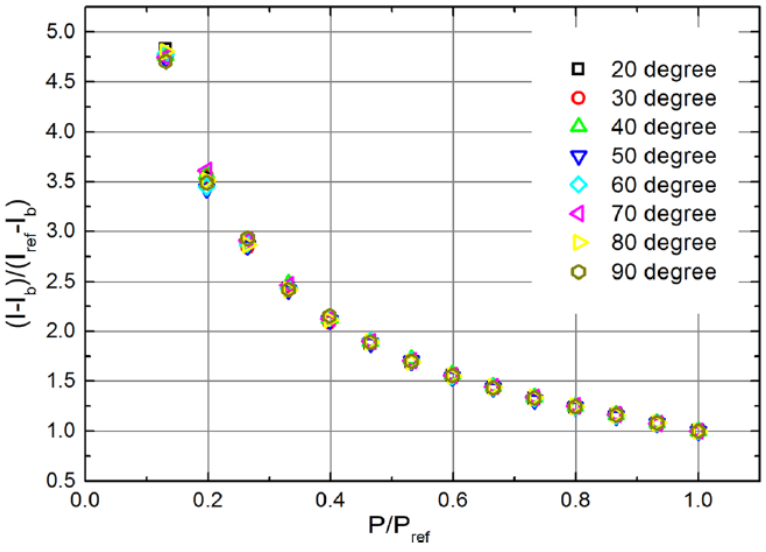

Figure 6. PSP calibration at different angles (Reprinted from Shiau et al. [6])

3.3 Test Matrix

To study the parametric effect of coolant to mainstream mass flow on two different vanes for comparison, a total of 6 experiments were carried out as shown in Table 1. The mainstream to coolant density is kept as unity by using nitrogen as coolant.

Table 1: Summary of test conditions for two vanes

Experiment #	MFR %	Design
1	3.12	Vane 1
2	3.82	Vane 1
3	4.61	Vane 1
4	3.12	Vane 2
5	3.82	Vane 2
6	4.61	Vane 2

3.4 Experimental Uncertainty

The main factor contributing to the uncertainty is the intensity of the PSP recorded by the camera. By using the method of Kline and McClintock [20], the uncertainty of the film cooling effectiveness at $\eta = 0.1$, 0.3, and 0.6 is 15%, 4.5%, and 3% respectively, in the current study. In addition, there is a 2-3% uncertainty in coolant mass flow caused by the measurement of coolant flow through the orifice meter. To have more accurate test results, 100 images are recorded and averaged in each test case. Tests are also repeated to ensure repeatability.

3.5 Results and Discussion

3.5.1 Pressure Distribution

Figure 7 shows the static pressure (P_s) distribution contours (normalized with inlet total pressure (P_t)) on the vane surfaces. In order to have more detailed information about the pressure distribution and the corresponding flow field, radial and streamwise averaged static pressure information is also provided in Fig. 7. The top figure shows the streamwise pressure distributions. The black, red, and green lines are taken at radial locations near the inner ring, center line, and outer ring, respectively. To provide the streamwise distribution, the pressure is averaged over a small region in the radial direction. The pressure is averaged 15-25%, 45-55%, and 85-95% for the inner, center line, and outer locations, respectively.

Similarly, for all the three views, the radial pressure distribution from the outer ring (y/H= 0) to the inner ring (y/H= 1) is shown next to each contour in form of the streamwise averaged pressure. For the pressure side view, the static pressure is averaged from SH1-SH6 for the leading edge portion (vertical dashed black line). For the rest of the pressure surface, the average is carried out at for P2-P3 (vertical dashed red line), P3-P4 (vertical dashed green line), and P5-P6 (vertical dashed magenta). A similar approach for the suction side surface is adopted with the average between S1-S2 (vertical black dashed line), S2-S3 (vertical red dashed line), S3-S5 (vertical black dashed line), and S5-TE (vertical red dashed line).

The detailed static pressure distribution provides insight into the coolant distribution over the vane surfaces. A closer look at the radially averaged curves (above

the contours) for the pressure surface reveals that the static pressure is slightly higher near the inner ring followed by the midspan and then the near the outer ring. The higher static pressure near the inner endwall becomes clearer by looking at the radial static pressure distribution (see line plot on the left of pressure surface contour). This could be due to the formation of different vortices (primarily the pressure side vortex) near the inner endwall. Due to higher static pressure at the inner ring region, it is expected that the coolant ejecting from the near inner endwall holes will be lower as compared to the rest of the cooling holes on the pressure surface.

The pressure distribution on the suction surface on the other hand has an opposite trend as that on the pressure surface. Both the radial and streamwise averaged curves reveals that the static pressure near the inner endwall region is lower as compared to the midspan and the outer ring region. Therefore, the cooling holes near the inner ring are expected to eject more coolant compared to the midspan and outer ring regions. In addition, a local high-pressure spot can be seen on the suction surface for $x/L > 0.6$. This is mainly due to the passage vortices produced near the suction surface.

The pressure distribution on the vane surfaces shows the robustness of the pressure sensitive paint. The PSP gives detailed information of how the pressure is varying from the inner to the outer ring as well as from the leading edge to the trailing edge of the vane. This aids to calculate the detailed film effectiveness on the entire vane surface which otherwise is not possible since the cooling holes are closely packed with the possibility of conduction heat transfer using traditional heat transfer experiments.

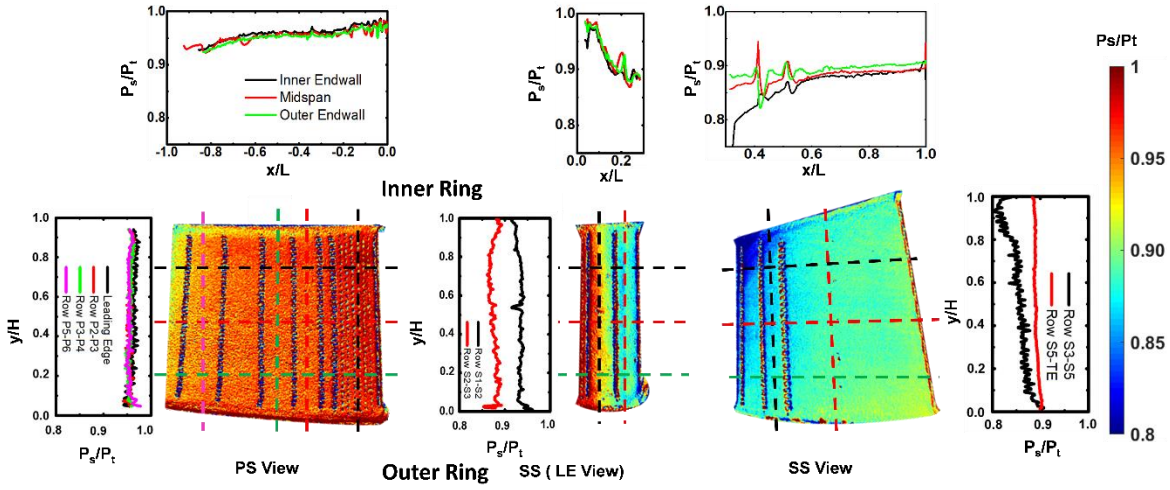

Figure 7. Static Pressure Distribution

3.5.2 Coolant Distribution & Split

The film cooling effectiveness contours for PS, SS (LE View), and SS (SS View) for vane 1 and vane 2 at all the coolant to mainstream mass flow ratios are given in Fig. 8. In terms of coolant distribution, the coolant is distributed non-uniformly for both the pressure and the suction surface from the inner ring to the outer ring. This non-uniform coolant distribution can be attributed to the pressure distribution on the vane surface. Similar coolant distribution patterns are witnessed for vane 1 and vane 2 are witnessed in the radial and streamwise direction.

For the pressure surfaces of vane 1 and vane 2, non-uniform coolant coverage is seen from the outer ring (y/H=0) to the inner ring (y/H=1). In general, for both vanes, the pressure surface cooling holes near the inner ring have less coolant compared to the midspan and the outer ring cooling holes. This behavior is witnessed for the showerhead

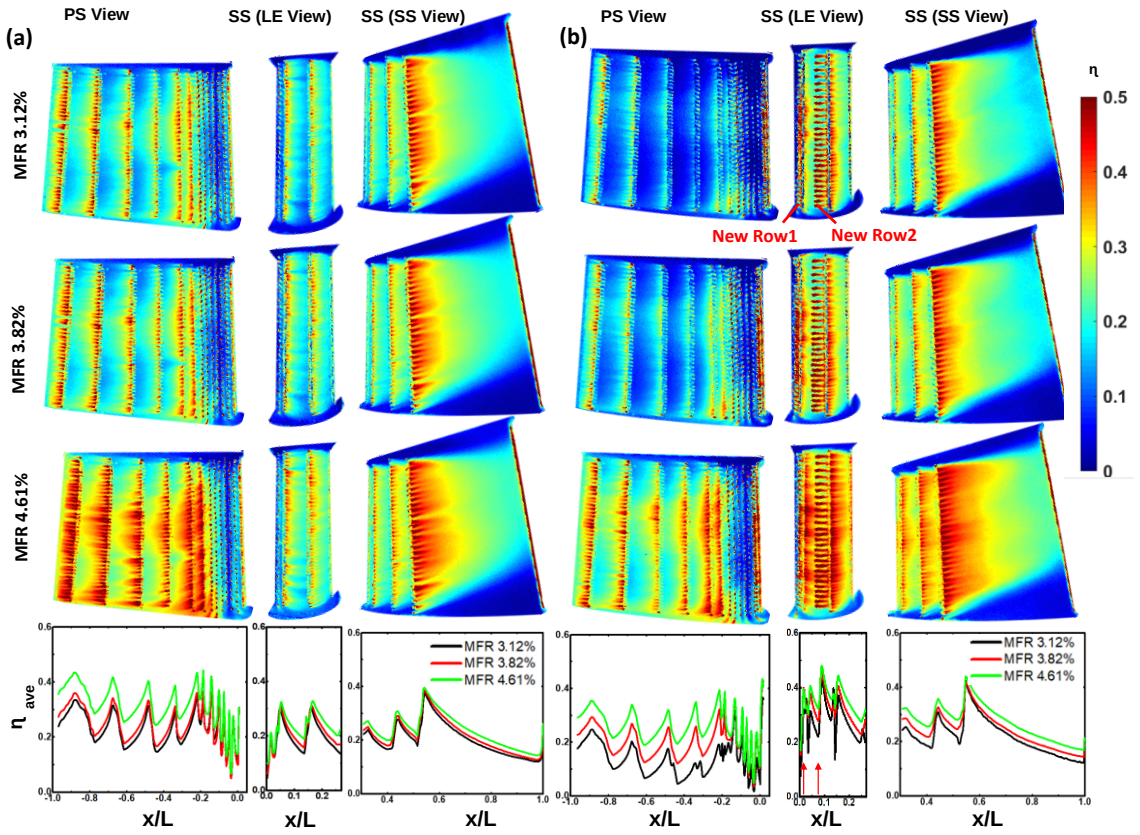

Figure 8. Film effectiveness contours and spanwise averages for vane 1(a) and vane 2 (b)

holes (SH1-SH6) and pressure side holes (P1-P6). The reason for this is a relatively higher mainstream static pressure on the vane pressure surface near the inner ring. The suction surface, on the other hand, has a reverse trend as compared to the pressure surface for both designs. In general, more coolant is seen near the inner ring holes due to relatively lower mainstream static pressure, as compared to the mid span and outer ring cooling holes. This is clearly seen in the vane 1 design for all the rows (S1-S5). However, for vane 2, R3-R5 show similar behavior as that for vane 1 but for R1-R3, the midspan region has more coolant coverage. This is due to the addition of the new row 1. New row 1 has a cluster of holes near the mid span region. Coolant from this cluster carries over to R2 and R3 and

possibly further to R4 or R5. Thus, overall, the coolant distribution on the suction surface for vane 2 is slightly different from vane 1 due to additional rows. Furthermore, the suction surface has coolant converging to the center of the vane surface for both cooling designs. This is primarily due to local high-pressure zones near the inner and outer ring (for x/L > 0.6). The converging nature of coolant on the suction surface is well documented in the open literature [11-13].

The coolant split between the pressure and suction surfaces is also important information that will help to understand the film effectiveness comparison between the pressure surface and the suction surface. This will also help in comparison of both vane designs and how the addition of new cooling holes helps in coolant distribution. An estimate of coolant ejecting from each row of holes is provided in Table 2 for both vanes. To estimate the amount of coolant to each row of holes, a constant discharge coefficient is assumed for all the holes (0.7 for cylindrical and 0.9 for fan shaped holes [21]). With the external static pressure (Ps) known from the PSP and the plenum pressure (Pc) measured using pressure taps, the actual mass flow through each hole can be calculated using,

$$\dot{m} = C_d \sum_{i=1}^{N} \sqrt{2\rho_c [Pc - Ps]} \frac{\pi}{4} d^2 \qquad (3)$$

The actual mass flowing through each row of holes can be used to estimate the local coolant velocity in order to estimate the local blowing ratio at each row of holes. The

estimated coolant mass flow and blowing ratio at each row of holes for vane 1 and vane 2 at MFR=3.82% is tabulated in Table. 2.

For vane 1 pressure surface, the showerhead holes consume an estimated 0.45% of the coolant while rest of the pressure surface consumes 0.93% of coolant. This accounts for a total of 1.38% of coolant being utilized by the pressure surface. The showerhead holes although consuming a significant amount of coolant, still have, lower effectiveness as compared to the rest of pressure surface (see Fig. 8). This is because the showerhead holes have vertical cylindrical holes compared to shaped holes on the pressure surface (P1-P6). The showerhead holes provide significant internal cooling to the leading edge region due to the high amount of coolant. The suction surface of vane 1 has almost an equal amount of estimated coolant (0.17%) ejected from each row of holes with the last row (S5) having 0.40% of coolant. Since S5 is expected to provide coolant to the majority of the suction surface, it is designed to eject a significant amount of coolant to the remaining cooling holes. A total of 1.08% of coolant is ejected from the suction surface while 1.14% of coolant is ejected though the trailing edge of the vane surface. A cursory view of Fig. 8(a) shows that the pressure surface of vane 1 has an overall higher film effectiveness as compared to the suction surface which can be contributed to the uneven split of coolant between the pressure and suction surfaces.

Coolant estimation for vane 2 is also provided in Table 2. With the introduction of two new rows, an overall reduction in coolant on the pressure surface is estimated while an increase in coolant to the suction surface is estimated. The total estimated coolant to the pressure surface is now 1.13% while that to the suction surface is 1.30%. The coolant

distribution almost reverses with the suction surface having more coolant. This can be observed on a cursory view of Fig. 8(b). A higher overall film effectiveness on the suction surface can be seen. It is important to note that the coolant estimation through each row of holes may not exactly correspond to the film effectiveness at each row on both surfaces. One of the major reasons could be the difference in local pressures within each cavity of the vane which could be different from the measured plenum pressure. The plenum pressure, on the other hand, is measured using pressure taps and is assumed to be the same for the complete plenum.

The local blowing ratio values are also provided in Table 2. Due to the lower mainstream static pressure on the suction surface as compared to the pressure surface, a higher estimated coolant mass flux is observed on that surface. However, the local blowing ratio in those regions is lower as compared to the region where that the external pressure is high. As a result, the suction surface has lower local blowing ratios as compared to the pressure surface. Similarly, the local blowing ratio decreases in the streamwise direction from the leading edge to the trailing edge. The leading edge holes, however, have low blowing ratios compared to the rest of the holes because of cylindrical holes. It is also interesting to see that the introduction of two new rows of holes on the vane 2 suction surface results in an overall decrease in local blowing ratios due to lower plenum pressure

Table 2: Cooling hole locations and coolant flow rates and blowing ratios at different rows for MFR=3.82%

	x/L	MFR% (V1)	MFR% (V2)	M (V1)	M (V2)
TE	-0.98				
P6	-0.82	0.20	0.16	0.72	0.66
P5	-0.65	0.20	0.16	0.72	0.66
P4	-0.46	0.17	0.15	0.86	0.78
P3	-0.32	0.12	0.10	0.87	0.80
P2	-0.20	0.12	0.10	0.87	0.80
P1	-0.18	0.12	0.10	0.87	0.80
SH6	-0.14	0.075	0.06	0.65	0.59
SH5	-0.09	0.075	0.06	0.65	0.59
SH4	-0.07	0.075	0.06	0.65	0.59
SH3	-0.04	0.075	0.06	0.65	0.59
SH2	-0.02	0.075	0.06	0.65	0.59
SL	0	--	--	--	--
SH1	0.001	0.075	0.06	0.65	0.59
New S1	0.016	NA	0.15	NA	0.65
S1	0.04	0.17	0.16	0.70	0.65
New S2	0.089	NA	0.14	NA	0.57
S2	0.14	0.17	0.15	0.60	0.57
S3	0.27	0.17	0.15	0.60	0.57
S4	0.41	0.17	0.16	0.60	0.55
S5	0.52	0.40	0.39	0.57	0.53
TE	0.99	1.14	1.06	NA	NA

3.5.3 MFR effect on film effectiveness

Figure 8 also shows the film effectiveness in the streamwise direction radially averaged from the inner to the outer ring. As the MFR is increased, longer traces of film are observed in the streamwise direction for both designs, resulting in better film effectiveness. Thus, a positive MFR effect is witnessed for both vane designs. This is more evident on the pressure surface of the two vanes. Since the pressure surface is a concave

surface, almost all the coolant is captured by the vane with minimum coolant lift-off, resulting in a significant increase of film effectiveness from lowest to highest MFR. The suction surface for vane 1, however, does not show a significant increase in film effectiveness with the increase in MFR. This could be due to the convex shape of the suction side surface resulting in some coolant lift-off at higher MFR due to relatively higher coolant momentum. Nonetheless, a positive trend in film effectiveness is witnessed for the current range of MFR in the study. However, the suction surface for vane 2 has a significant increase in film effectiveness with increase in MFR. This is due to the two new rows of holes which have a carryover effect to the downstream suction surface.

The vane flow field is highly three dimensional with a dominant passage vortex that rises from the corner of the leading edge and travels all the way to the suction surface. The effect of this vortex is quite visible on the suction side with both the hub and tip of the vane remaining unprotected. This occurs for all MFR. The study by Shiau et al. [6] on the endwall of the same test vanes revealed that the higher MFR (around 4%) effects the flow field (suppression of horseshoe vortex) on the vane surface causing the coolant jet to change its behavior in the streamwise direction. This, however, is not the case in the current study where even the highest MFR of 4.81% is not changing the flow field. The coolant seems to be following the same pattern in the stream wise direction. One reason could be the local low blowing ratios (see Table. 2), making it difficult for the coolant jets to interact with the mainstream flow to alter the flow field. It is worth studying to know if even higher MFR in the current test section can alter the flow field and a better film coverage on the suction surface can be obtained by suppression of the passage vortices.

3.5.4 Radially averaged film effectiveness comparison

The film cooling effectiveness comparison for both vanes is provided in Fig. 9. A clear shift in coolant distribution can be seen (as discussed in section 3.5.2). The film effectiveness in the leading edge region, or the showerhead holes (x/L=0 to x/L=-0.13), for vane 1 varies between an 0.2 to 0.3 from lowest to highest MFR. The vane 2 design, on the other hand, has a varying value from 0.1 to 0.2. Similarly, a drop in effectiveness is witnessed for the pressure surface (x/L=-0.14 to x/L=-0.98) for vane 2 compared to vane 1. This drop in is significant at the lowest MFR (the effectiveness drops from average value of 0.25 from vane 1 to 0.12 for vane 2). At the highest MFR, the effectiveness drops from around 0.35 for vane 1 to 0.28 for vane 2. The significant drop at lower MFR could be due to lower plenum pressure for vane 2 compared to vane 1, which makes it difficult for the coolant to eject onto the high-pressure surface. This indicates that by having an extra row of holes not only affects the suction surface, but also has a significant impact on the pressure surface. It is evident from the film effectiveness on the pressure surface for both vanes that the coolant has been redistributed. Naturally a high film effectiveness is expected on the suction surface of vane 2 since the suction surface has two additional rows of fan shaped holes. Figure 9 shows a clear increase in film effectiveness for vane 2 compared to vane 1 for the suction surface. This increase in effectiveness is more pronounced for x/L<0.2. This is the region where the new row of holes is located (marked by red arrows in Fig. 9). For all MFR ratios, a systematic increase in film effectiveness is witnessed for vane 2 compared to vane 1. A maximum increase in effectiveness can be

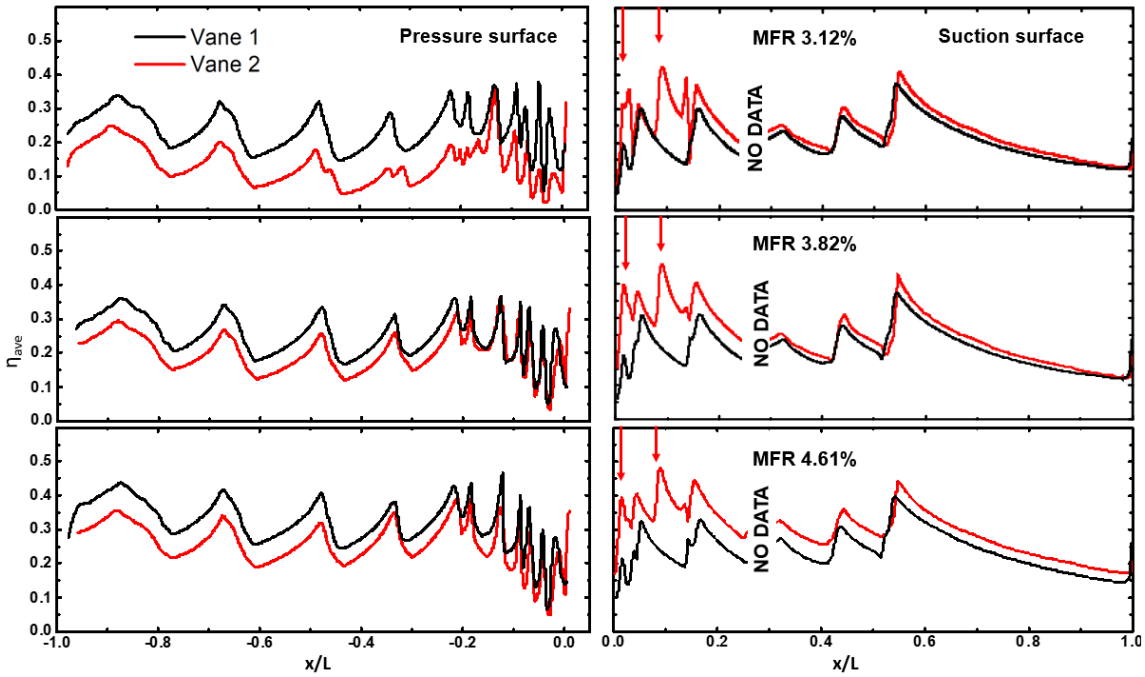

Figure 9. Comparison of radially averaged film cooling effectiveness for both vanes at all coolant flow rates

seen from 0.25 for vane 1 to 0.40 for vane 2 at the highest MFR. It is also interesting to see that the two additional holes have carry over of coolant to R3-R5 (x/L>0.2) on the suction surface, resulting in an overall better film effectiveness for the new design.

With both designs having their own advantages, vane 1 seems to be more protected on the pressure surface while vane 2 is generally more protected on the suction surface. However, the pressure distribution on the suction surface reveals a sudden change in pressure for x/L< 0.2. This pressure drop dictates a sudden increase in velocity on the vane surface. Therefore, the mainstream gas with high temperature can cause more damage to this region if it is not well protected. The two additional holes for vane 2 seem to play a positive role in re-distributing the coolant and providing protection to the high-speed region on the suction side surface; however, coolant to the pressure surface is sacrificed.

3.5.5 *Area averaged film effectiveness comparison*

The area averaged effectiveness shown in Fig. 10 gives a direct comparison for the vanes. Vane 1 has higher pressure side area averaged effectiveness than the suction surface at all MFR values. In addition, a significant increase in effectiveness with MFR can be seen on the pressure surface compared to the suction surface. Vane 2, on the other hand, has a higher suction effectiveness as compared to the pressure surface.

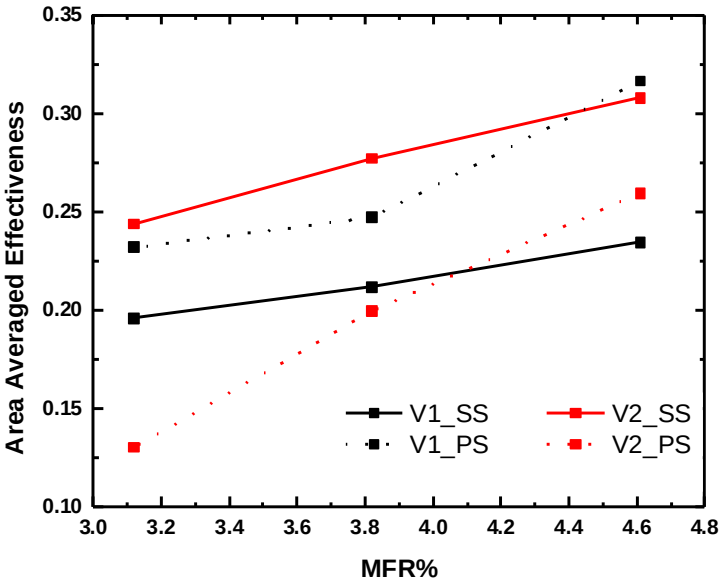

Figure 10. Area averaged film effectiveness

4. INFLUENCE OF COOLANT DENSITY ON TURBINE BLADE TIP FILM COOLING AT TRANSONIC CASCADE FLOW CONDITIONS USING THE PRESSURE SENSITIVE PAINT TECHNIQUE*

4.1 Literature Review

Within the gas turbine, the tips of high-pressure blades experience the highest thermal loads of any component within the engine. One of the many reasons is the leakage flow across the blade tip gap from the blade pressure side to the suction side. The accelerating leakage flow yields high heat transfer coefficients, which compromises the durability of the blades. Therefore, many experimental and numerical studies of blade tip cooling designs are available in the open literature which feature the complicated flow field near the blade tip and the effect of different parameters like blade tip design, blowing ratio and density ratio.

Han [1] provided a review for many experimental blade tip studies including a variety of plane tip and squealer tip designs. The advantages of placing cooling holes on the tip surface or the near tip pressure side surface for different injection cases is well documented. For instance, Ahn et al. [22] used a 5-blade linear blowdown wind tunnel to experimentally study a plane tip design with both tip and pressure side injection. The blowing ratio was varied from 0.5 to 2.0 and a positive blowing ratio effect was reported

*Reprinted with permission from Ullah, I., Alsaleem, S., Wright, L., Shiau, C., and Han, J., 2021, "Influence of Coolant Density on Turbine Blade Tip Film Cooling at Transonic Cascade Flow Conditions Using the Pressure Sensitive Paint Technique." ASME. J. Thermal Sci. Eng. Appl. Copyright ASME 2021

for different coolant injection cases (pressure side only, tip only, and tip and pressure side together). Kwak and Han [23, 24] studied a plane tip as well as a squealer tip design in the same facility and recorded different coolant injection scenarios from the tip as well as the pressure side holes. Results suggested by introducing film cooling holes on the tip and the pressure side surface gives better film cooling effectiveness and reduces the over-tip leakage flow and heat transfer coefficients. A positive blowing ratio effect was also reported. Similarly, Mhetras et al. [25] further investigated the film cooling effectiveness of shaped holes on the near tip pressure side and cylindrical holes on a blade tip surface. The pressure sensitive paint (PSP) measurement technique was used to measure the film cooling effectiveness as well the surface pressure of the blade tip. They concluded that M=1.0 and M=2.0 provided the highest film cooling effectiveness and that the blowing ratio has a positive impact on the film effectiveness. A similar study by Narzary et al. [26] was carried out at transonic conditions on a squealer tip blade with pressure side hole injection at very high blowing ratios (M=1-4). A positive impact of the pressure side injection holes was seen at all blowing ratios.

Two interesting studies were also done by Christophel et al. [27, 28]. These papers experimentally studied the film cooling and heat transfer of a plane blade tip by blowing coolant through pressure side holes and tip holes. This test was carried out in a low-speed wind tunnel. A baseline design with no coolant blowing was compared with coolant blowing from the pressure side as well as the tip holes. The coolant blown from the pressure side changes the flow field on the tip surface. Results suggested a slight local increase in heat transfer but an overall performance improvement was observed with the

introduction of pressure side holes. A similar conclusion was also obtained by Kim and Metzger [29] in their experimental study. They concluded that significant protection from heat transfer can be provided to the tip by introducing cooling holes near the pressure side corner of the tip. Rezasoltani et al. [30] performed an experimental and numerical study of turbine blade tip film cooling effectiveness under rotating conditions. They reported that the overall film effectiveness increases with blowing ratio (from M=0.5 to M=1.25) for both the plane tip and squealer tip. It was also concluded that the film effectiveness increases with rotational speed (RPM=2000 to 3000) for the plane tip but decreases for the squealer tip. Other studies [31, 32] were carried out recently with tip and pressure side hole injection on a rotating blade. A positive effect for coolant blowing was again witnessed.

Apart from the effect of different cooling injection cases on the film effectiveness, researchers have also tried to quantify the flow field on the tip surface as well as the leakage flow across the tip. Azad et al. [33], for instance, used a 5-blade linear blowdown facility to experimentally investigate a plane tip design with different tip clearances. Results showed that the over-tip leakage flow can be reduced by decreasing the tip clearance. The pressure measurements near the tip and shroud provides information about the leakage flow across the tip and form the basis for future tip designs to reduce the tip leakage. Similar studies by Bindon [34] and Moore et al. [35] give a general understanding of tip leakage flow patterns and the general flow field around the blade tip. Key and Arts [36] and Naik et al. [37] experimentally and numerically studied film cooling and heat transfer of different blade tip designs including a flat tip at transonic conditions. The flow

field over the blade tip was very well captured using oil flow visualization. Results suggested that PS injection helped to reduce the over-tip leakage. The aerodynamic loss for the squealer tip was recorded to be reduced as compared to a plane tip. Recently, Paty et al. [38] investigated the near tip and over-tip flow field characterized in the form of leakage mass flow distribution and aerodynamic field. This study carried out at engine representative conditions was based on different tip geometries. Arisi et al. [39] also completed a numerical study to characterize the aerothermal performance of a plane tip at different transonic conditions. They concluded that increasing the Mach number results in increased heat transfer over the tip surface. In addition, they observed that the heat transfer was primarily dominated by upstream crossflow at Mexit = 0.85. Zhang et al. [40] studied the over-tip shock structure caused on the tip surface at transonic conditions. The study revealed that the flow structure is deeply affected by the presence of shock wave on the tip surface causing a local variation in the heat transfer. One other study by Shyam et al. [41] also captures the tip heat transfer under transonic conditions and provides valuable suggestions.

The above-mentioned studies (and many others) in the open literature clearly show the coolant blowing ratio at different injection scenarios has a profound impact on the film effectiveness, heat transfer and the corresponding tip flow field. However, these studies use the density ratio of 1.0. The expected coolant-to -mainstream density ratio can be around 1.5 to 2.0 in engine conditions. The effect of higher density ratios on the blade tip film cooling needs to be quantified.

Studies of density ratio effect are very limited in the open literature. Jeong et al. [42] did study the heat transfer coefficients and film cooling effectiveness in a low speed, linear cascade at DR=1.0 and DR=1.5 and recorded a positive impact for the density as well as the blowing ratio. Therefore, it is imperative to parametrically study the combined effect of blowing and density ratio on the film effectiveness and the corresponding flow field. This study combines the effect of density ratio (DR=1.0, 1.5, and 2.0), blowing ratio (M=0.5, 1.0, and 1.5), and the tip and pressure side injection cases together to provide a more complete database for the blade tip film cooling design reference. In addition, the effect of blowing ratio and density ratio on the over-tip flow leakage is estimated for various tip injection designs for comparison.

4.2 Experimental Setup and Method

4.2.1 Three Blade Linear Cascade

Testing was carried out in a linear, three blade cascade installed in a blow down facility as shown in Fig.11. The inlet and exit Mach numbers of 0.29 and 0.75 were achieved at a steady state for 10 seconds. The mainstream velocity was measured by using pitot static probes at $0.5C_{ax}$ upstream and downstream of the leading and trailing edge. The overall pressure ratio ($P_{t,inlet}/P_{exit}$) was 1.49. Narzary et al. [26] previously measured the flow periodicity upstream and downstream of the test blade over two blade pitches. Flow periodicity upstream and downstream of the blade was checked by measuring the wall static pressure as a percentage of average, upstream (inlet) and downstream (exit) pressure, respectively. The upstream and downstream guide walls were adjusted to obtain the flow periodicity at the inlet and outlet. In addition, the blade loading curve was also

obtained using a squealer tip with a TE cutback test blade having 29 pressure taps uniformly distributed on the suction and pressure surfaces of the blade. The loading curve was measured at 50%, 75%, and 95% of blade span. The loading curve is also compared to a numerical prediction at 50% span [43]. The flow periodicity and the loading curve are shown in Fig. 12(a) and Fig. 12(b), respectively. A square grid was used at $3.2C_{ax}$ upstream of the blade leading edge to create turbulence. A uniform turbulence intensity of 13.5% was measured at $0.5C_{ax}$ upstream of the blade. Details on the test section can be found in the previous study [26].

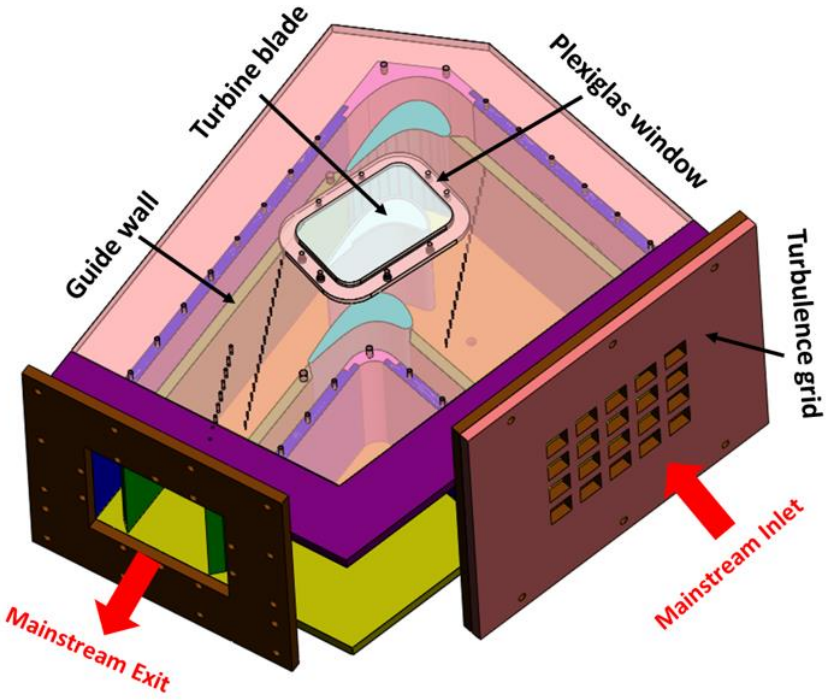

Figure 11. Turbine blade tip test facility

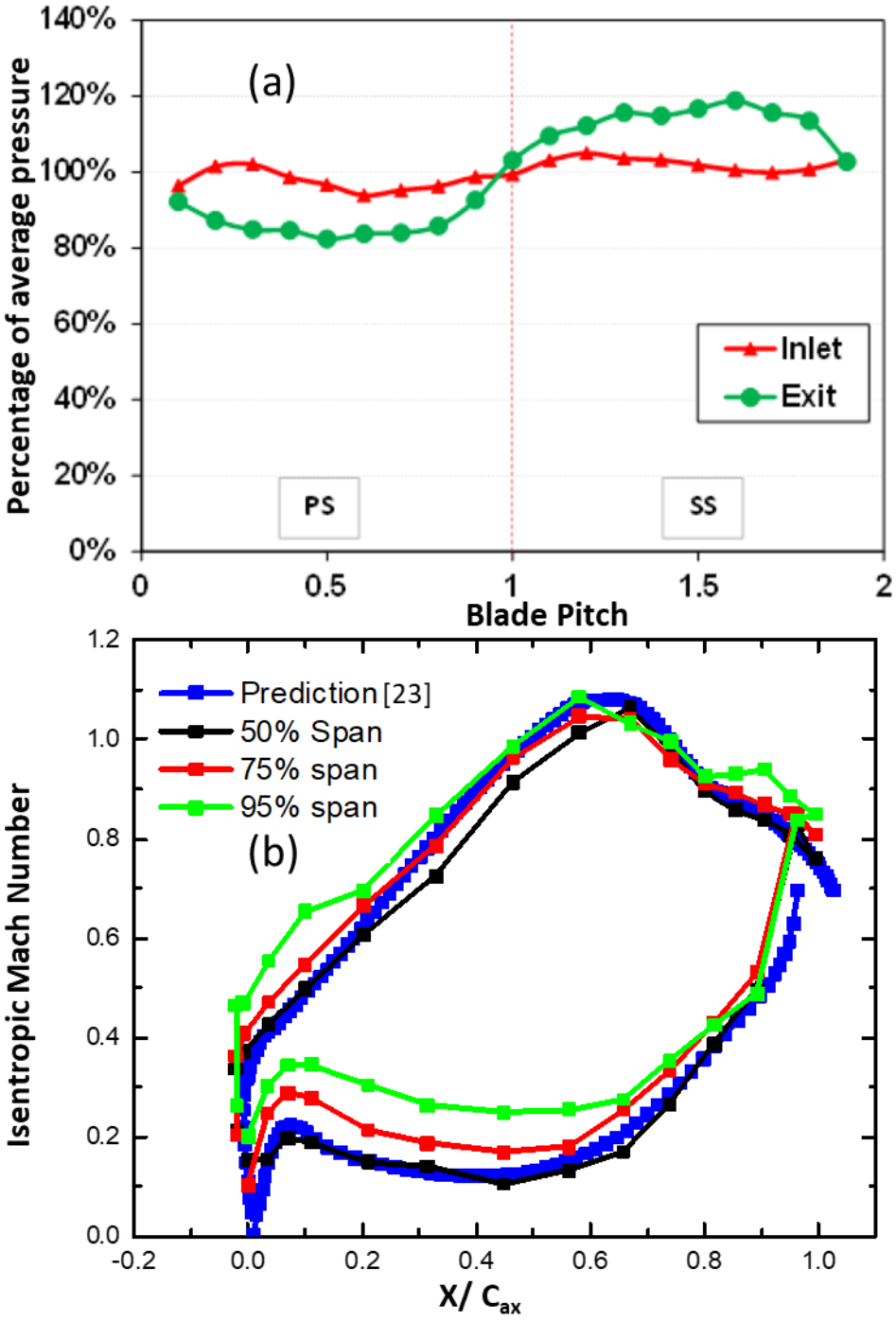

Figure 12. (a) Flow periodicity chart (Reprinted from Narzary et al. [26]) (b) Blade loading curves

4.2.2 Film Cooling System

A separate 3D printed test blade core was used to test the flat blade tip designs as shown in Fig.13. The blade core was fabricated from an SLA plastic material (PerFORM) with 0.1 mm build layers. The blade tip, however, was fabricated from the same material with a high resolution 0.05 mm build layer to acquire quality data. The blade tip, as shown in Fig. 13(a), was designed to have 15 near tip pressure side shaped holes with a 45^o-45^o compound angle configuration and p/d=12.68. The distance of the PS holes from the tip edge is 8.9 mm. For the tip surface, 15 vertical cylindrical holes were equally spaced (at a distance of 5.33 mm from the PS edge) along the pressure side with p/d=12.83 and l/d=6. The tip gap (h) is 2.2 mm. Details of the PS and tip cooling holes can be found in Fig. 14. The blade core, as shown in Fig.13(b), is divided into two zones in order to maintain a uniform average blowing ratio at the tip for each zone. Figure 13(c) shows the top of the flat tip design with the tip holes and PS holes lying in two different zones. Two different flow meters were used to supply the coolant to each zone. Three different types of foreign gases were used to study the density ratio effect: N_2 (DR = 1.0), CO_2 (DR = 1.5), and Argon/SF_6 mixture (DR = 2.0). For all the tests, the mainstream and coolant temperatures were maintained at 20° C.

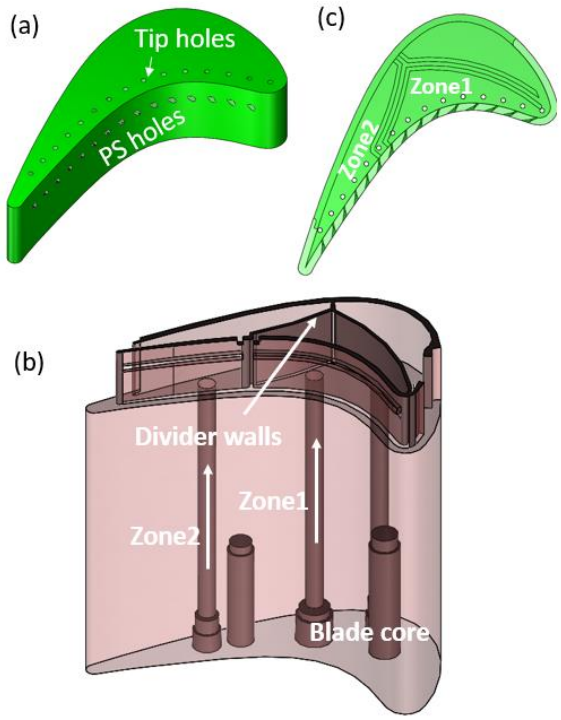

Figure 13. (a) Blade tip design (b) Blade core (c) Blade tip top cross-sectional view

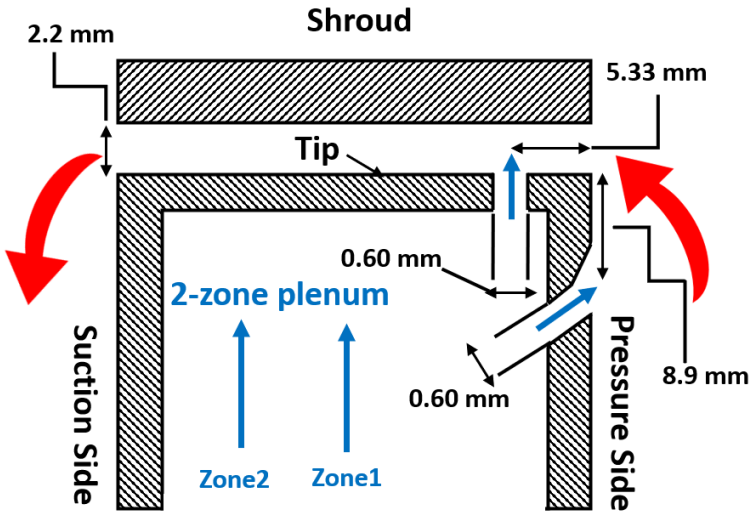

Figure 14. Geometry of film cooling holes

4.2.3 Experimental Method – Pressure-Sensitive Paint

The experimental method used for this test is the same as that for the three-vane annular cascade in section 3.2.3.

4.3 Test Matrix

To study the parametric effect of blowing ratio and density ratio on tip film cooling effectiveness, 36 experiments were carried out. These experiments were divided into four coolant injection scenarios. (a) The first test scenario is the tip only injection (top view). This test has coolant injected from the tip cooling holes only with average blowing ratios of M=0.5, 1.0, and 1.5. For each flow condition, an average blowing ratio for each zone is assumed (for a desired flow condition) first. Then the local mainstream mass flux is calculated at each hole by using the tip surface pressure distribution from the PSP. The total mainstream mass flux for each zone is then calculated by adding and averaging the local mainstream mass flux at each hole. Finally, using the averaged mainstream mass flux and assumed average blowing ratio value for a given zone, the coolant mass flux/flow rate is then calculated at the given blowing ratio. (b) The second testing scenario is a shared PS & tip injection (top view). This test has coolant injected from the tip holes as well as from the PS holes. But the amount of coolant (mass flow rate) is the same as that of tip only injection (case (a)). In other words, the same coolant amount as that of tip only injection is shared by the tip and the PS holes. This test scenario will be referred as PS & Tip (shared) in the rest of the paper. (c) The third scenario is the PS & tip injection (top view) but with M=0.5, 1.0, and 1.5 coolant blowing both from the tip as well as from the PS holes separately (i.e. the coolant flow for this case is almost double the amount of

coolant for the tip only injection). This scenario will be referred as PS & Tip (separate) in the rest of the paper. (d) The fourth scenario is PS & tip injection (angled view) with M=1.0, 1.5, and 2.0 coolant blowing from the tip as well as from the PS holes separately but with an angled view. This case is similar to case (c), but images are captured from the side to view the PS holes. To control the blowing ratio of coolant during the test, an approximate 4-6 seconds steady state time is achieved. During this time the test data is taken. It is also worthy to mention that before an actual test for a given flow condition, 2-4 tests are carried out to adjust the blowing ratio during the steady state time period. Once the coolant flow is set correctly using the flow meter, the actual test is then carried out for data taking. The density ratio is varied from DR=1.0-2.0 to study the effect of density ratio. Table 3 summarizes all the tests carried out. The momentum flux ratios for different flow conditions are also tabulated in Table 4. To study the parametric effect of blowing ratio and density ratio on tip film cooling effectiveness, 36 experiments were carried out.

Table 3: Summary of test conditions for blade tip testing

Injection case		Blowing Ratio	Density Ratio
(a) Tip only Top View		**0.5, 1.0, 1.5**	**1.0, 1.5, 2.0**
(b) PS & Tip (shared coolant) Top View		**0.5, 1.0, 1.5**	**1.0, 1.5, 2.0**
(b) PS & Tip (separate) Top View	**PS**	**0.5, 1.0, 1.5**	**1.0, 1.5, 2.0**
	Tip	**0.5, 1.0, 1.5**	
(c) & Tip (separate) Angled view	**PS**	**0.5, 1.0, 1.5**	**1.0, 1.5, 2.0**
	Tip	**0.5, 1.0, 1.5**	

Table 4: Momentum flux ratios

Injection case	M	$I_{DR=1.0}$	$I_{DR=1.5}$	$I_{DR=2.0}$
Tip Only	0.5	0.25	0.17	0.13
	1.0	1.0	0.67	0.5
	1.5	2.25	1.5	1.13
PS & Tip (shared)	0.5	0.13	0.09	0.07
	1.0	0.56	0.37	0.28
	1.5	1.57	1.05	0.79
PS & Tip (Separate)	0.5	0.25	0.17	0.13
	1.0	1.0	0.67	0.5
	1.5	2.25	1.5	1.13

4.4 Experimental Uncertainty

The variation in the mainstream pressure and coolant flow meter exit pressures contributes to around ±2% of uncertainty of the mainstream and coolant flow rates. However, the main factor contributing to the uncertainty is the intensity of the PSP recorded by the camera. By using the method of Kline and McClintock [20], the uncertainty of film cooling effectiveness at η = 0.1, 0.20 and 0.40 is 15%, 9%, and 4.5%, respectively, in the current study.

4.5 Results and Discussion

4.5.1 *Tip Only Injection*

The film cooling effectiveness distributions for tip only injection (top view) are presented in Fig. 15. The overall blowing ratio at a given flow condition is calculated by averaging the local blowing ratio for each cooling hole. In general, placing the cooling holes near the pressure side on the tip surface gives good coolant coverage on the tip. The coolant tends to cover most of the tip and follows the leakage flow direction from PS to

SS. At very low blowing ratios (M=0.5) and for all density ratios, little or no coolant is ejected from the first few holes near the leading edge of the blade. This is due to very high static pressure near the leading edge of the blade. For higher blowing ratios (M>0.5), the coolant trace is visible and clearly covers the majority of the tip surface.

Figure 16 represents the laterally averaged film cooling effectiveness with $X/C_{ax}=0$ at the leading edge of the blade. A positive density ratio effect is seen for all blowing ratios as shown in Fig. 16(a). The positive density ratio effect is more significant at M=1.5 as compared to M=0.5 and M=1.0. The positive density ratio effect can be explained in terms of the momentum flux ratio ($I=M^2/DR$) of the coolant (see Table 4). At higher blowing ratios, the lower density coolant has higher momentum which yields less deflection by the leakage flow. This results in lower film effectiveness. The denser coolant on the other hand, has a lower momentum, which causes more coolant deflection towards the tip surface due to the leakage flow. This results in better film coverage. A positive blowing ratio effect is also seen as shown Fig. 16(b). However, M=1.0 seems to be the optimum blowing ratio for all the density ratios. As the tip holes are cylindrical and vertical holes, the coolant is not easily deflected in the direction of the leakage flow. This effect is more prominent for M>1.0 and DR=1.0. This is because the momentum flux ($I=M^2/DR$) of the coolant is very high. This trend agrees with the trend reported by Mhetras et al. [25] for a blade tip with cylindrical holes. Figure 17 shows the area averaged effectiveness for the tip only injection cases for all blowing ratios. The area averaged effectiveness increases from 0.04 to 0.09 as the coolant density increases from DR=1.0 to DR=2.0 at M=1.5. This is almost more than twice the increase in effectiveness for the same amount of coolant.

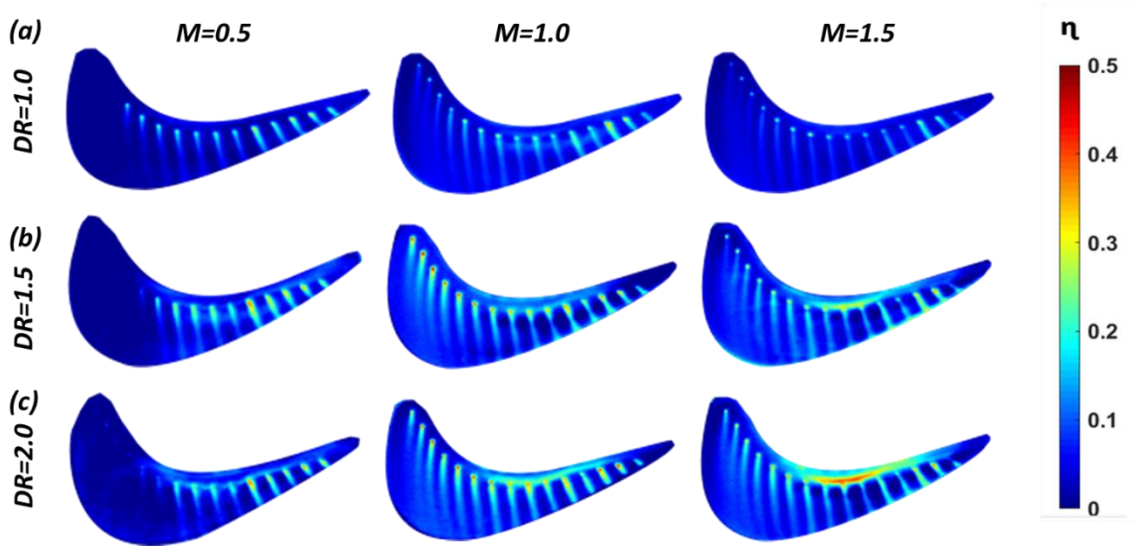

Figure 15. Film cooling effectiveness distributions (top view) for tip only injection at all density ratios

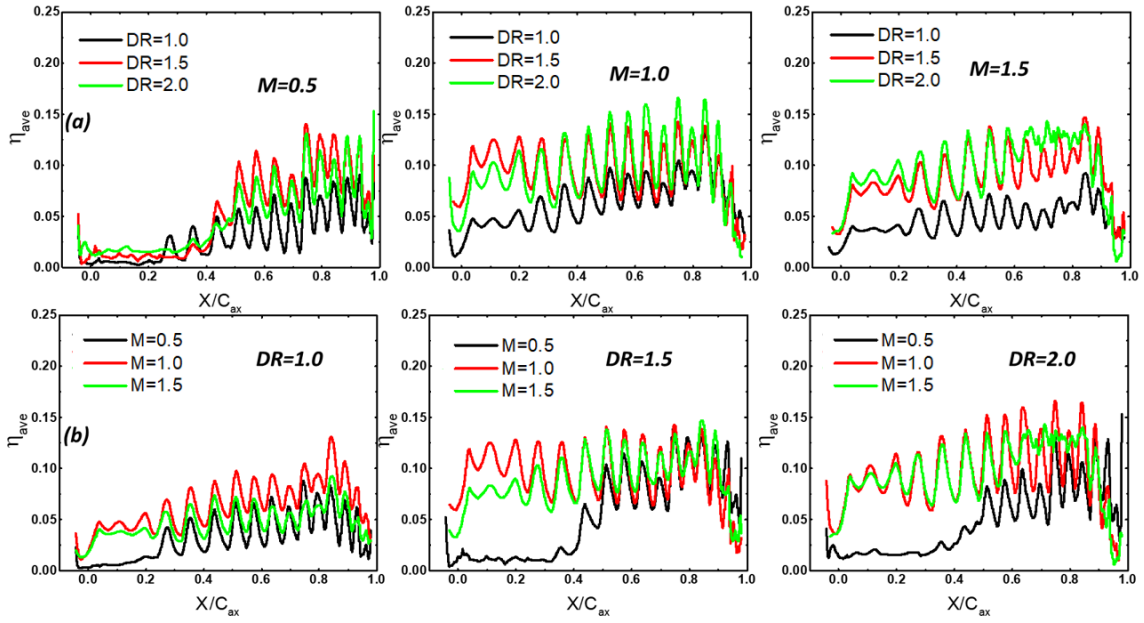

Figure 16. Laterally averaged film cooling effectiveness for tip only injection at all density ratios

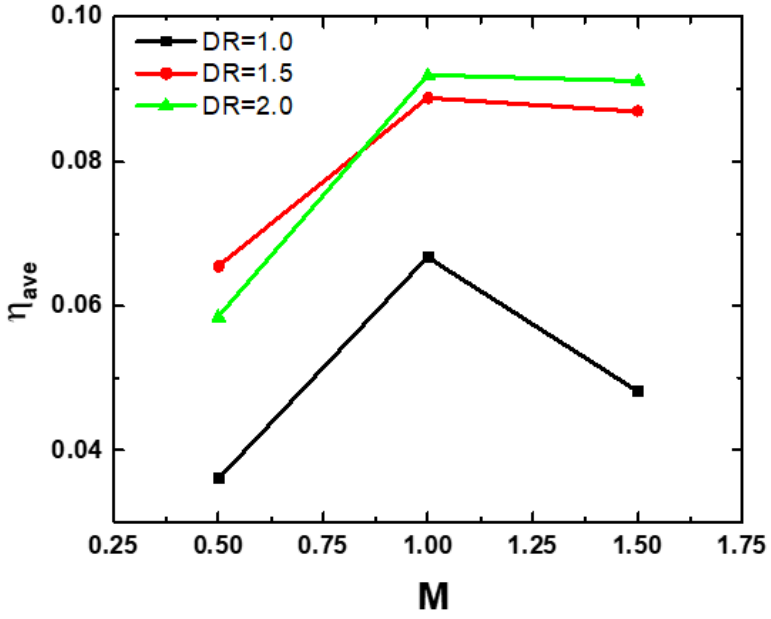

Figure 17. Area averaged effectiveness for tip only injection

4.5.2 PS & Tip Injection (Shared)

As shown in the previous section, for vertical cylindrical holes, higher momentum coolant (M=1.5) is not able to provide good film coverage due to less deflection in the direction of the leakage flow. In order to reduce the momentum of the coolant to experience favorable deflection, the blowing ratio can be reduced while maintaining the same amount of coolant. Therefore, it is interesting to observe if the same amount of coolant as that of the tip only injection case is supplied with the PS & tip holes open at the same time. It will also provide a fair comparison for fixed mass flow rates. By keeping the same amount of coolant as the tip only injection scenario, the coolant is almost equally shared by the tip holes and the PS holes. The actual tip blowing ratio for this case is thus less than the tip only injection case. For tip only injection blowing ratios of M=0.5, 1.0, and 1.5, the corresponding blowing ratios (on the tip) for the PS & tip shared injection are

M≈0.35, 0.75, and 1.25, respectively. Figure 18 shows the distributions for all the blowing ratios of PS & tip (shared) injection. It should be noted that the blowing ratios mentioned in Fig. 18, Fig. 19, and Fig. 20 are the blowing ratios for tip only injection. Mentioning the tip only injection blowing ratios in these figures implies that for a given tip only injection blowing ratio (mentioned in the figure), the same amount of coolant is also injected with PS & tip holes open.

Overall, a better film coverage can be seen for all the blowing ratios at all density ratios. Although the same amount of coolant is now split between the PS and the tip holes, the average blowing ratio at the tip is now lower which helps in reducing coolant momentum. In addition, some of the coolant from the PS side carries over to the tip helping to increase effectiveness. Figure 19 represents the laterally averaged effectiveness at different blowing ratios for DR=1.0, 1.5, and 2.0 for the tip only injection and PS & tip (shared) injection. In general, the PS & tip injection case yields better effectiveness. It is also interesting to see that by opening the PS holes, a better film coverage is observed near the leading-edge (X/Cax < 0.4) area of the tip surface at a low blowing ratio (M=0.5). The area averaged effectiveness curves, as shown in Fig. 20, provide a direct comparison. For all density ratios at M=0.5, PS & tip injection gives better effectiveness due to low and sufficient momentum of the coolant as compared to tip only injection. It seems none of the coolant is injected to the PS side due to high static pressure on the pressure surface. At M=1.0, for DR=1.0 and DR=1.5, the PS & tip injection show low effectiveness as compared to tip only injection. This could be due to some of the coolant being injected to the PS holes. At an even higher blowing ratio (M=1.5), the tip only injection case has more

coolant momentum. This results in lower effectiveness for tip only injection as compared to PS & tip (shared) injection case.

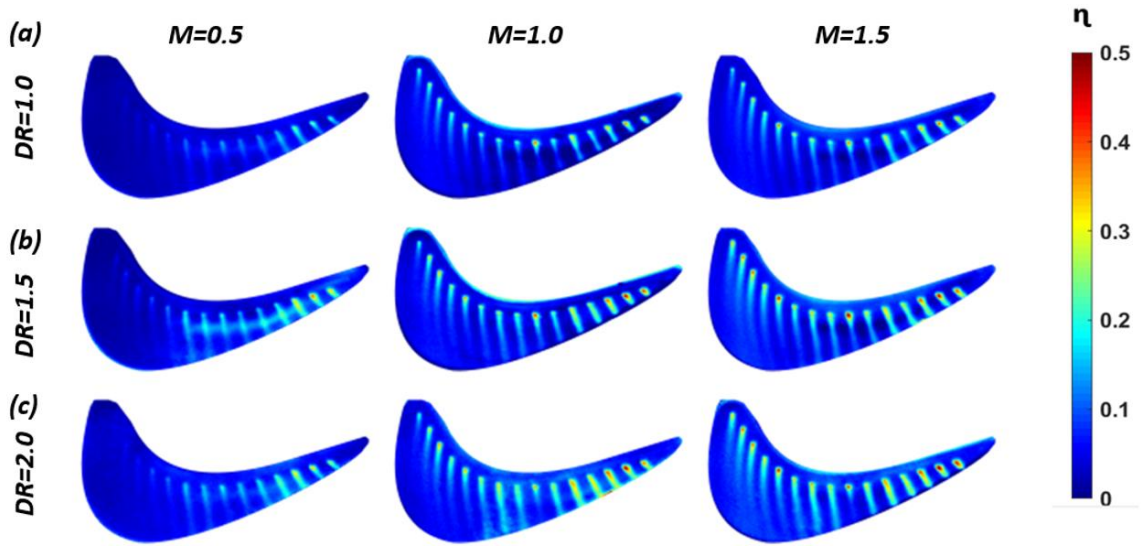

Figure 18. Film cooling effectiveness distributions (top view) for PS & tip (shared) injection at all density ratios

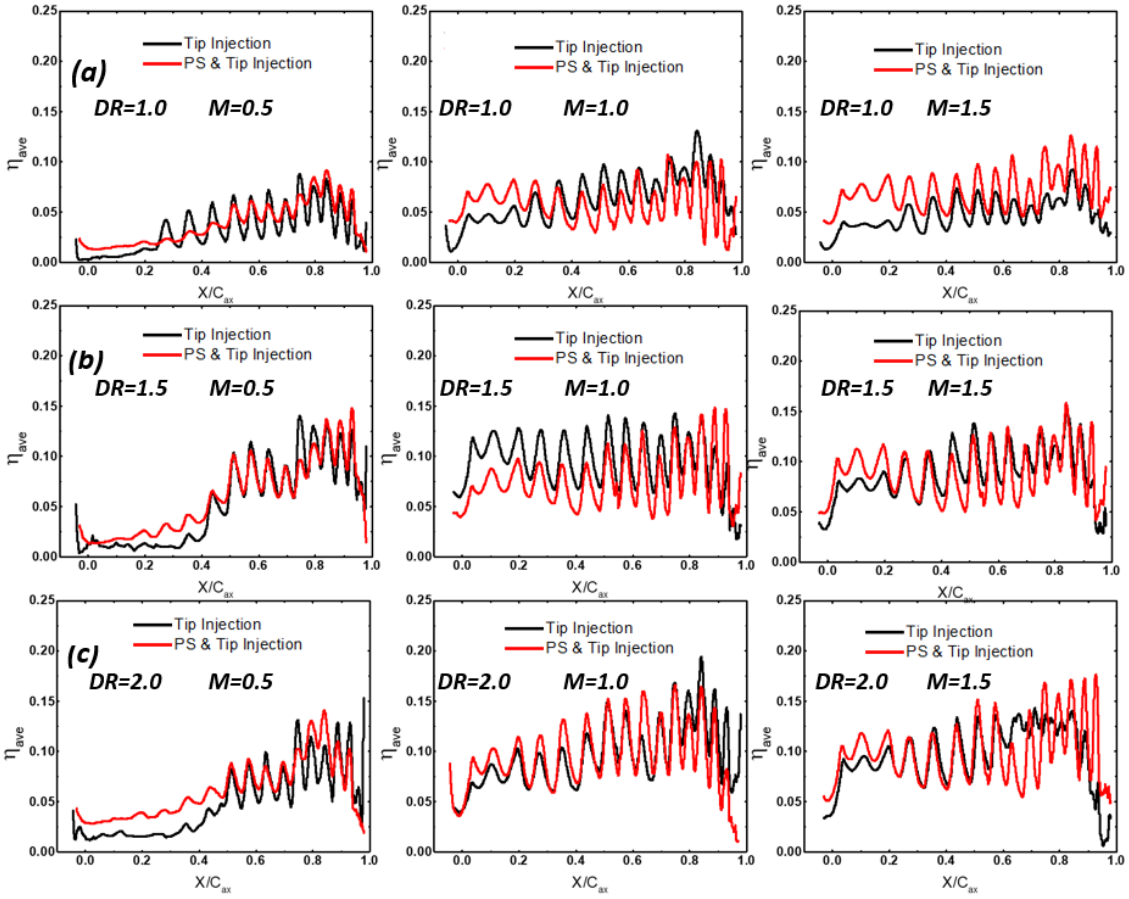

Figure 19. Laterally averaged film cooling effectiveness for tip only vs PS & tip (shared) injection

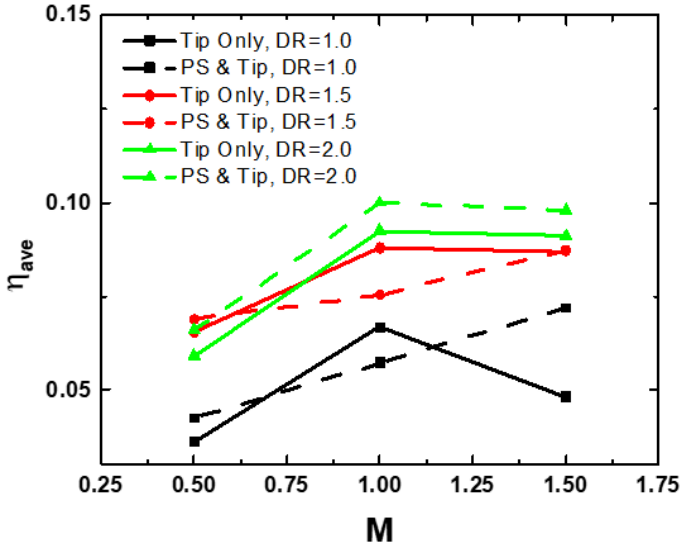

Figure 20. Area averaged effectiveness for tip only vs PS & tip (shared) injection

4.5.3 PS & Tip Injection (Separate)

As far as the film effectiveness is concerned, keeping the PS holes open improved the film coverage. Therefore, it is beneficial to study the same injection scenario with the same blowing ratio at the PS and tip holes. With the PS & tip holes now open, coolant is injected through both PS holes and tip holes with M=0.5, 1.0, and 1.5 separately. Figure 21 shows the distributions for all density ratios. Similar behavior is observed as in the previous case. However, due to the presence of more coolant (almost double) as compared to the tip only injection and PS & tip (shared coolant) injection cases, a more uniform film coverage and higher film effectiveness is seen at all the blowing and density ratios. Figure 22 shows the blowing ratio and density ratio effects for this case. A positive density ratio and blowing ratio effect is witnessed with M=1.0 as the optimum blowing ratio. Figure 23 shows the area averaged effectiveness for all the coolant injection cases. An optimum blowing ratio of M=1.0 is witnessed for all density ratios. The density ratio effect for PS

& tip (separate) is also similar to the previous scenarios i.e. at the same blowing ratio, DR=2.0 provides double the effectiveness as DR=1.0.

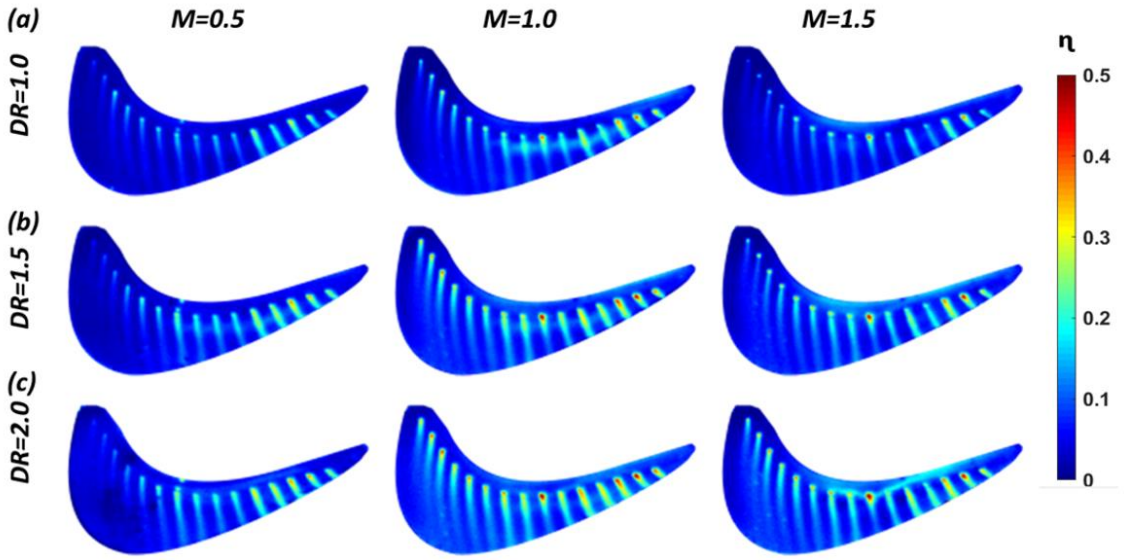

Figure 21. Film cooling effectiveness distributions (top view) for PS & tip (separate) injection at all density ratios

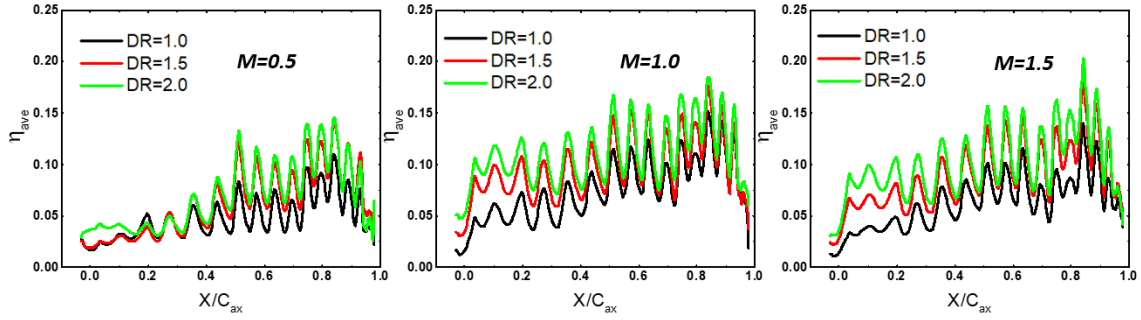

Figure 22. Laterally averaged film effectiveness for PS & tip (separate) injection for all densities

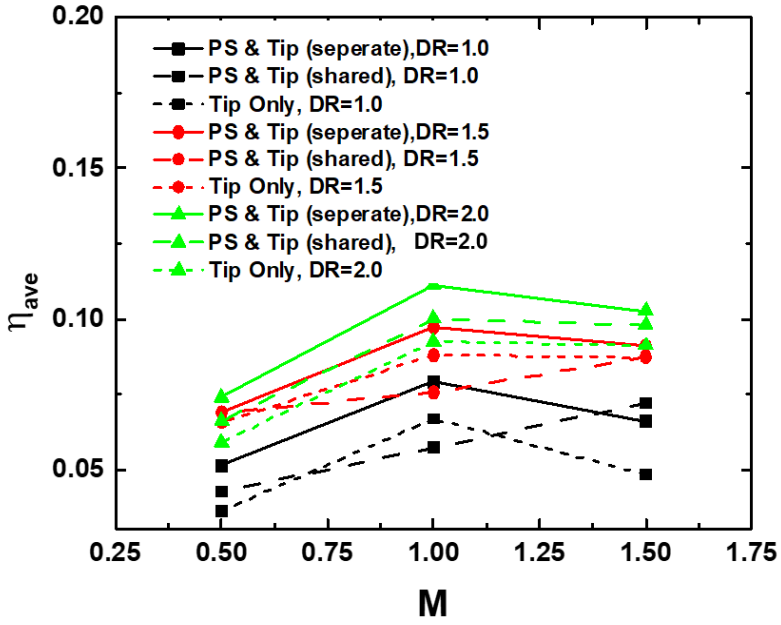

Figure 23. Area averaged effectiveness for PS & tip (separate) injection

4.5.4 PS & Tip Injection (Separate) – angled view

It was necessary to study the perspective view of the test blade with PS and tip holes open for select blowing ratios in order to get the appreciation for the PS holes. Figure 24 shows the contours (angled view) for PS & tip injection (separate) for total blowing ratios of M=1.0, 1.5, and 2.0. The blowing ratio effect for the PS holes is positive for all the density ratios because coolant lift off is not significant for the compound shaped hole. In addition, the coolant sticks to the PS surface due to the mainstream flow direction. The density ratio effect is negative at M=1.0 due to insufficient momentum at high densities. However, for M>1.0, the density ratio effect is clearly positive due to lower but sufficient momentum of the heavier density coolant as compared to DR=1.0. The PS injected coolant does provide coverage on the PS surface; however, the coolant seems to follow the

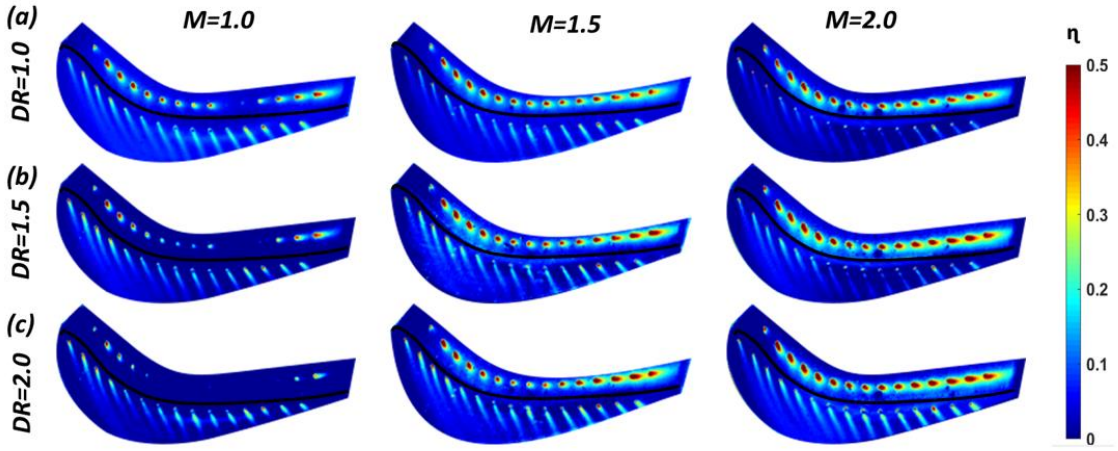

Figure 24. Film cooling effectiveness distributions (angled view) for PS & tip (separate) injection

direction of the mainstream. Very little coolant is seen to carry over to the tip surface as seen in the top views of Fig.15, Fig.18, and Fig.21. This might be due to the fact that the PS holes were placed too far below the pressure side tip edge of the blade.

4.5.5 Leakage Flow

Apart from the film effectiveness, leakage flow is one of the important aspects in gas turbine blades. To quantify the leakage flow for the current blade tip design and to parametrically study the effects of blowing and density ratios in different injection scenarios, a simple orifice model is assumed for compressible flow. The actual mass flow through an orifice for a compressible flow is given in equation 4:

$$\dot{m} = h\sum_{x=0}^{Cax} C_d P_t \left(\frac{P_s}{P_t}\right)^{\frac{\gamma+1}{2\gamma}} \sqrt{\frac{2\gamma}{(\gamma-1)RT_m}\left[\left(\frac{P_t}{P_s}\right)^{\frac{\gamma-1}{\gamma}} - 1\right]}\Delta x \qquad (4)$$

C_d in the above equation is assumed to be 0.7. h is the tip gap which is equal to 2.2 mm. P_t is the total inlet pressure measured by the pitot probe while P_s is the local static pressure measured on the PS rim (measured from the tip holes to the PS edge) by the PSP. By

measuring the P_s/P_t data locally at a position x with width Δx and a constant tip gap h, the local mass flow leakage is calculated. Total mass flow leakage is then equal to the summation of local mass flow leakages from X/C_{ax}= 0 to X/C_{ax} = 1. As a general rule of thumb, a higher P_s/P_t means lower leakage flow.

Figure 25 shows the static pressure distribution without coolant injection while Figure 26 shows the static pressure distribution for (a) tip only injection (b) PS & tip injection (shared) injection and (c) PS & tip injection (separate) injection at DR=1.0. These contours provide the general idea about the flow field behavior on the tip surface. Figure 27 shows the static pressure ratio quantitatively (laterally averaged on the PS rim). From Figure 25, 26 and 27, as a general trend, the static pressure is highest at the leading edge of the tip and decreases moving downstream from LE to TE. A very low-pressure zone is witnessed between X/C_{ax}=0.5 to X/C_{ax}=0.8. This is where the mass flow leakage is the highest. This is a typical flow field reported by Ahn et al. [22] and Arisi et al. [39]. A cursory view of the contours also reveals that the static pressure for tip only injection, as shown in Fig. 26(a), is higher than the PS & tip (shared) coolant injection case shown in Fig. 26(b). This means less leakage with the tip only injection. This could be due to low actual blowing ratio on the tip for the PS & tip (shared) injection case as compared to the tip only injection. The coolant momentum does not seem to be enough to block the leakage flow as compared to tip only injection. When the amount of coolant is almost double i.e. the same blowing ratio is maintained at the PS & tip holes as shown in Fig. 26(c), the static pressure increases and the leakage flow is reduced. Now the tip has the same blowing ratio of coolant as that of the tip only injection.

The total mass flow leakage as a percentage of the mainstream flow is presented in Table 5. With no coolant injection, the leakage flow is 1.93%. However, when coolant is injected, a minimum amount of leakage of 1.67% is calculated. This accounts for a 12% decrease in leakage flow. A similar phenomenon of reduction in leakage flow (by tip holes near the PS rim) is also reported by Kim and Metzger [29]. As a general trend, the leakage flow for tip only injection and PS & tip injection (separate) yields the minimum leakage. The PS & tip injection with shared coolant blowing from the PS and the tip holes have higher leakage as compared to the latter cases but the difference is not significant. Additionally, the density ratio effect on the leakage is insignificant but a positive blowing ratio effect is witnessed. The PS holes seems to have little or no effect on the leakage flow for the current study. As discussed with Fig. 24, coolant from the PS holes does not carry over to the tip, rather it flows in the direction of the mainstream. PS holes do not appear to reduce the leakage flow. This may be because the PS holes are too far below the pressure side tip edge in the current design. However, whether or not the PS holes have any effect on the leakage flow at even higher blowing ratios is a question that remains unanswered.

It is important to note the leakage flow estimation has an assumed Cd value of 0.7; however, this value can vary from hole to hole and for different flow conditions. Ideally, the magnitude of the discharge coefficient should be varied as necessary. In the current setup, there is no direct way to estimate Cd on the tip at different flow conditions. The results could also be biased to assume different values for Cd at different flow conditions. Therefore, a constant coefficient for all the flow conditions provides a consistent comparison. To explore the sensitivity of the discharge coefficient on the leakage

calculation, a change in Cd from 0.65 to 0.75 was considered. Over this range, the estimated leakage flow varies approximately 8%. Therefore, the use of Cd = 0.7 for all holes provides a reasonable approximation of the leakage flow across the tip of the airfoil.

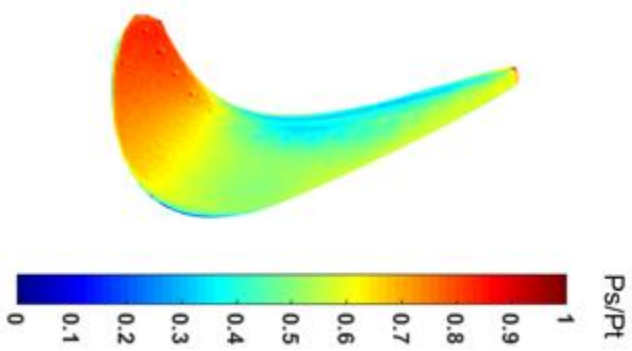

Figure 25. Static pressure distribution on blade tip with no coolant

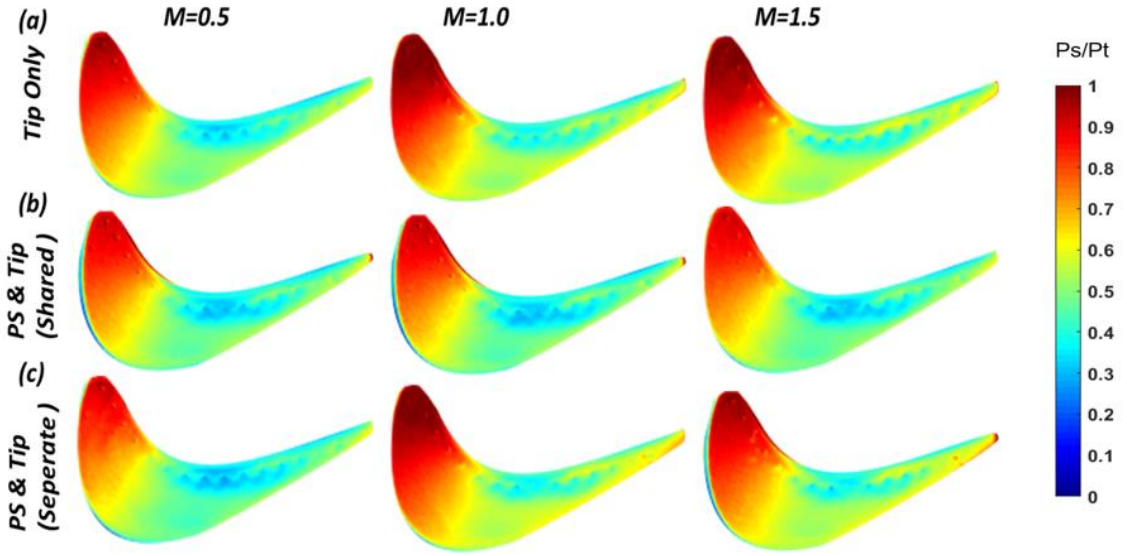

Figure 26. Static pressure distribution (top view) for all injection scenarios at DR=1.0

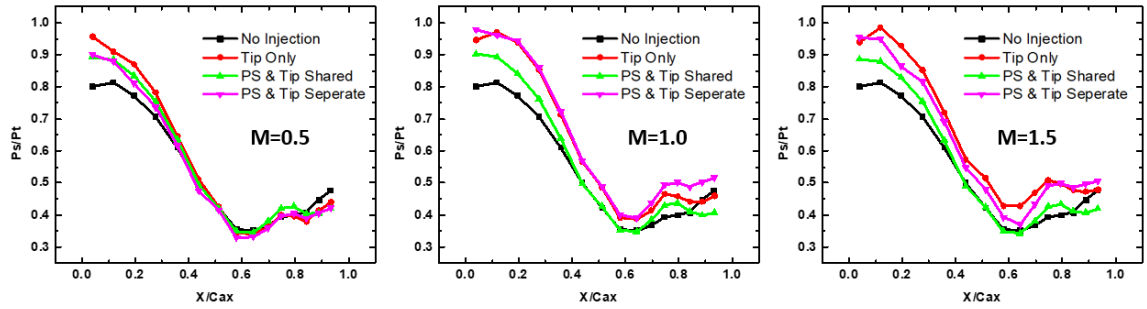

Figure 27. Laterally averaged static pressure distribution on the PS rim of the tip at DR=1.0

Table 5: Leakage flow as a percentage of mainstream passage flow for all injection cases

Injection case	Tip only			PS & Tip (shared)			PS & Tip (separate)		
DR	**1.0**	**1.5**	**2.0**	**1.0**	**1.5**	**2.0**	**1.0**	**1.5**	**2.0**
No coolant					**1.93%**				
M=0.5	**1.77%**	**1.73%**	**1.74%**	**1.85%**	**1.85%**	**1.85%**	**1.85%**	**1.85%**	**1.85%**
M=1.0	**1.69%**	**1.78%**	**1.73%**	**1.84%**	**1.73%**	**1.73%**	**1.67%**	**1.73%**	**1.73%**
M=1.5	**1.70%**	**1.76%**	**1.76%**	**1.86%**	**1.79%**	**1.80%**	**1.77%**	**1.79%**	**1.80%**

5. FILM COOLING AND AERODYNAMIC PERFORMANCE OF PRESSURE SIDE CUTBACK AND ALTERNATING DISCHARGE FOR BLADE TRAILING EDGE COOLING

5.1 Literature Review

Studies have been carried out on the trailing edge (TE) of a turbine blade focusing on different configurations to better protect this region. One of the most commonly studied designs is the pressure side cutback trailing edge design. Researchers have identified many parameters that directly or indirectly affect the TE film cooling effectiveness for a pressure side cutback design. Among others, these parameters include cooling passage size, trailing edge thickness, lip thickness, slot height, and internal cooling design,. Sivasegaram et al. [44] studied the effect of lip thickness-to-slot height ratio on film cooling by testing two different lip thicknesses-to-slot height ratios of 0.80 and 1.60. They concluded that film cooling is inversely related to lip thickness. Mukherjee [45] studied the influence of blowing angle and lip geometry on the film effectiveness of a slot. The effect of blowing angle and lip thickness was documented in the form of correlations. Taslim et al. [46] also did a very fundamental study on slot film effectiveness. Parameters including density ratio, lip thickness-to-slot height, blowing ratio, and slot width-to-height ratio were varied. Film effectiveness was strongly affected by the lip thickness and blowing ratio while all the other parameters did not affect the effectiveness significantly. This study forms the basis for many other studies in terms of the validation of data. A correlation was also developed relating the lip thickness and blowing ratio to the film effectiveness.

Holloway et al. [47, 48] studied trailing edge slot injection under realistic engine conditions. They observed the generation of periodic vortex shedding for larger lip thickness which accelerated the decay of the film effectiveness. Martini et al. [49, 50] also completed a fundamental study on a pressure side cutback trailing edge design by varying coolant blowing ratios from 0.2 to 1.1. They concluded the film effectiveness for the slot is significantly increased with an increase in blowing ratio in general. However, at a blowing ratio of approximately 0.6-0.8, the film effectiveness decreased with an increase in blowing ratio. This was due to the formation of vortex shedding. Cunha and Chyu [51] studied different types of TE configurations. They concluded the PS cutback design yielded the lowest temperatures as compared to the center line discharge design. They also documented the different parameters that affect the performance of a PS cutback design.

Choi et al. [52] carried out an experimental study in a low-speed wind tunnel on two different TE designs. They concluded that the design with a sloped land and shorter cutback slot provided better effectiveness compared to a zero sloped land and longer cutback slot. A negative blowing ratio effect was observed. Krueckels et al. [53] also studied the pressure side trailing edge and concluded that the effectiveness decreases with an increase in distance from the slot. Horbach et al. [54] showed the lip thickness has a pronounced impact on film effectiveness. A thicker lip resulted in intense unsteady vortex shedding downstream of the lip, resulting in more mixing and reduced effectiveness.

Gao et al. [55] also did an experimental study in a low-speed wind tunnel on different trailing edge cutback designs. They concluded a positive blowing ratio effect and

a negative lip thickness effect on the film cooling effectiveness for the slot. In addition to the slot film effectiveness, they also studied the film effectiveness on the land and sidewalls of the trailing edge cutback slot. The highest effectiveness was observed on the slots and sidewalls and the lowest was observed on the lands. Similarly, Ling et al. [56] also studied different cutback slot designs. These designs included straight land, medium tapered land, and strong tapered land. Strong tapered design recorded the highest film effectiveness. Furthermore, the land taper angle was recorded to have a significant impact on coolant concentration in the wake region downstream of the trailing edge. Wong et al. [57] also studied a baseline TE design and eight different internal cross corrugated TE slots. Exit shaping of the slots proved promising in terms of effectiveness improvement.

Parbat et al. [58] recently computationally studied three different TE designs. Two of these designs were the standard centerline discharge and PS cutback. A new design having a wavy structure at the TE was studied. This study revealed that better protection on the TE was achieved with this new design due to the redistribution of coolant to both the suction and pressure surfaces. The performance was more pronounced at a higher MFR. A positive MFR effect was observed for all the designs. Yan [59] also completed a computational study on a pressure side cutback design. The simulation agree with Martini's [49, 50] experimental results related to the complex vortex shedding caused at certain flow conditions and proved that the film effectiveness of a slot doest not vary monotonically with coolant flow rate.

Apart from film effectiveness, the pressure loss due to the TE design is an important factor that requires attention. Uzol et al. [60, 61], for example, studied the

impact of cutback length on the pressure loss characteristics. They studied two different cutback lengths (0 mm and 23 mm). They concluded that there is a strong interaction between the mainstream and the coolant ejected from the TE. This interaction creates a significant wake region downstream of the TE, resulting in pressure loss. The introduction of a cutback at the TE reduced the interaction between the mainstream and coolant and resulted in reduced pressure loss. Parbat et al. [58] also studied the aerodynamic losses for the standard PS cutback and the new way trailing edge design. They concluded that the new wavy TE design has 25% more loss as compared to the PS cutback design. The improved film cooling effectiveness comes at the expense of increased pressure loss through the passage.

The purpose of this study is to improve the wavy trailing edge concept with enhanced cooling on both the pressure and suction surfaces. With the new and improved version of the wavy trailing edge design, it is imperative to quantify also the aerodynamic performance. Therefore, the aerodynamic loss is studied and is compared with the standard PS cutback design. Since CFD has already been completed on the new wavy trailing edge design by Parbat et al. [58], this study is an experimental study of the same design and thus will confirm the trend from the numerical simulations.

5.2 Experimental Setup and Method

5.2.1 Five-Blade Linear Cascade

Experiments were conducted in a five-blade linear cascade test facility, as shown schematically in Fig. 28. Regions of interest are the pressure side and suction side of the TE for two different designs. The inlet and exit cross-sections of the wind tunnel are 19.6 cm (width) × 12.7 cm (height) and 12.9 cm (width) × 12.7 cm (height), respectively. The mainstream air is supplied by a centrifugal compressor which can provide a volume flow rate of up to 6.2 m3/s. A square bar turbulence grid with a bar width of 0.635 cm is placed 2.5 times of the axial chord length (C_{ax}) upstream of the center blade leading edge. The grid produces a measured turbulence intensity of around 10.5%. More details regarding the test section can be found in Chen et al. [62]. The cascade inlet and exit Mach numbers were 0.20 and 0.30, measured at $1.35C_{ax}$ upstream of the center blade leading edge and $1.47C_{ax}$ downstream of the center blade trailing edge, respectively, by a pitot-static probe. The cascade inlet and exit Reynolds numbers based on the axial chord length are 3.8×10^5 and 6.5×10^5, respectively. Pressure loss measurements are completed by traversing 10 pitot-static probes at $0.25C_{ax}$ downstream of the TE. Details of the mainstream conditions are given in Table 6. The loading curve for the blade [63] is also given in Fig. 29.

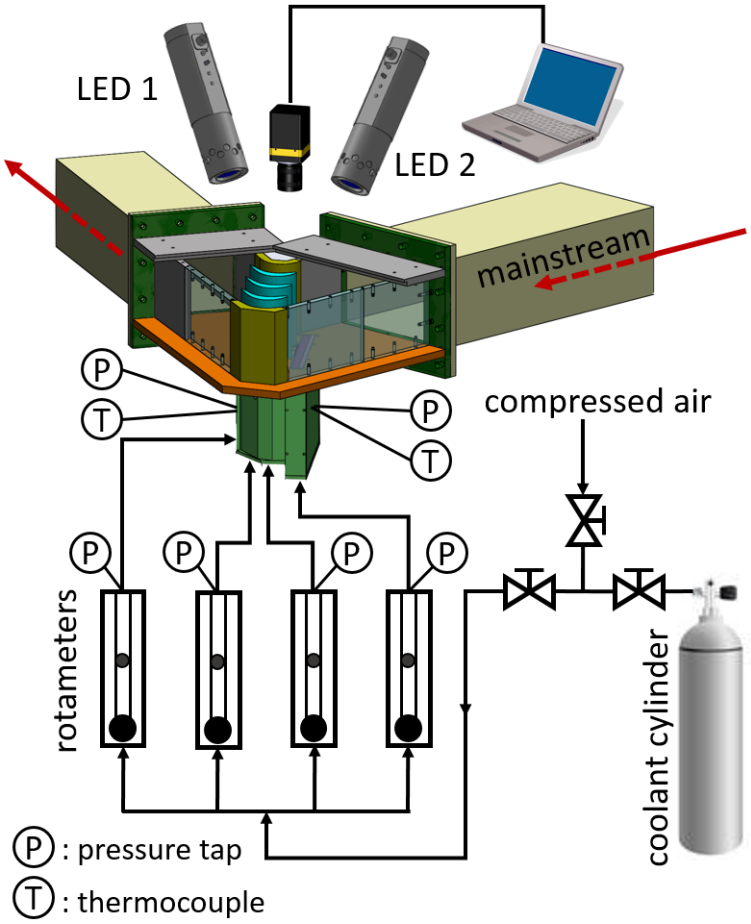

Figure 28. Five blade linear cascade (Reprinted from Chen et al. [63])

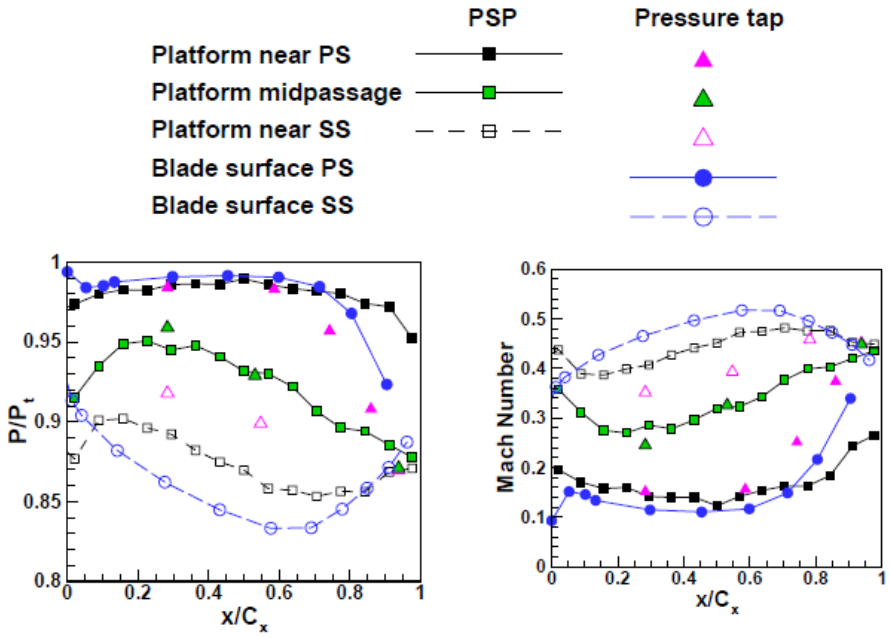

Figure 29. Loading curve for test blade (Reprinted from Gao et al. [64])

Table 6: Mainstream flow conditions for testing

Cascade Geometry			
Blade Height	**12.64 cm**	**Inlet Area**	**249 cm^2**
Axial Chord Length	**8.13 cm**	**Exit Area**	**164 cm^2**
Pitch	**7.69 cm**	**Inlet Angle**	**50.5 deg**
Total Turning Angle	**116.9 deg**	**Exit Angle**	**66.4 deg**
Mainstream Flow Conditions			
Inlet Ma	**0.20**	**Inlet Re**	**3.8 x 10^5**
Exit Ma	**0.30**	**Exit Re**	**6.5 x 10^5**
Tu %	**10.5**		

5.2.3 Film Cooling System

The test blades consist of two different designs. The first design is a pressure side cutback design. This design has cutback slots on the PS of the blade as shown in Fig. 30. A total of 39 cutback slots are present. The lip thickness-to-slot thickness ratio (t/s) is 1.04. The slot length is 5.3 mm. The thickness of the TE at the edge is 0.76 mm. Between the slots, the portion is called the land. In this particular design, the land portion is designed to be tapered. The sidewalls of the slots are also tapered. Detailed nomenclature can be found in Fig. 30.

The second geometry is the wavy trailing edge design, as shown in Fig. 31. The number of holes and the size of holes (s and d in Fig. 30) is kept the same while the PS cutback slots are replaced with a wavy-like structure. The wavy structure alternates between the pressure surface and the suction surface, thus, providing coolant to both surfaces. The thickness of the wavy structure at the edge is 0.26 mm. The wavy structure wavelength is 6.2 mm with an amplitude (A) of 0.75 mm. Detailed dimensions and definitions can also be found in Fig. 31.

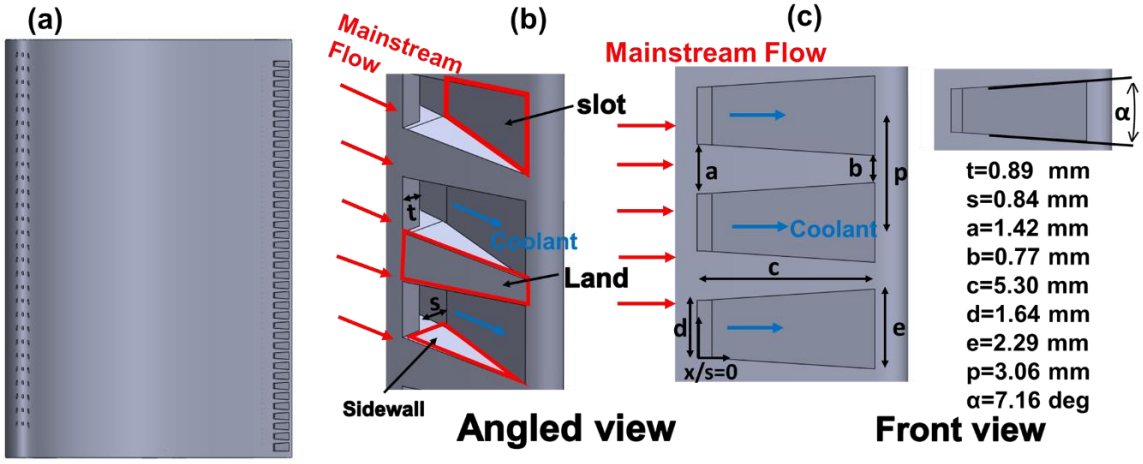

Figure 30. (a) PS Cutback Design view from pressure side, (b) (c) definitions and dimensions

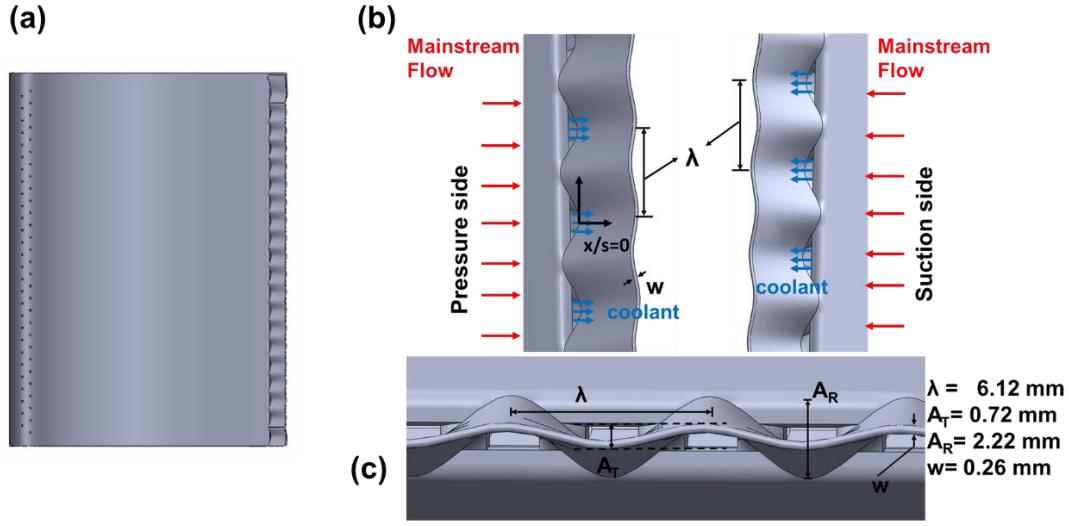

Figure 31. (a) Wavy Design view from pressure side, (b) (c) definitions and dimensions of the wavy structure

5.2.3 *Experimental Method – Pressure-Sensitive Paint*

The experimental method used for this test is the same as that for the three-vane annular cascade in section 3.2.3.

5.3 Test Matrix

To study the parametric effect of coolant-to-mainstream flow rate and density ratio on the trailing edge film cooling effectiveness, 30 experiments were completed. For each design, testing was completed at five MFRs (0.30%, 0.50%, 0.75%, 1.0%, and 1.25%) and three density ratios (1.0, 1.50, and 2.0). The corresponding blowing ratio for each MFR is provided in Table 7. The aerodynamic loss was also measured for both designs at DR=1.0.

Table 7: Summary of test conditions for two TE designs

Experiment #	MFR %	M	Design	Density Ratio
1-3	0.30	0.20	PS Cutback	1.0, 1.5, 2.0
4-6	0.50	0.35	PS Cutback	1.0, 1.5, 2.0
7-9	0.75	0.50	PS Cutback	1.0, 1.5, 2.0
10-12	1.00	0.80	PS Cutback	1.0, 1.5, 2.0
13-15	1.25	1.00	PS Cutback	1.0, 1.5, 2.0
16-18	0.30	0.20	Wavy	1.0, 1.5, 2.0
19-21	0.50	0.35	Wavy	1.0, 1.5, 2.0
22-24	0.75	0.50	Wavy	1.0, 1.5, 2.0
25-27	1.00	0.80	Wavy	1.0, 1.5, 2.0
28-30	1.25	1.00	Wavy	1.0, 1.5, 2.0

5.4 Experimental Uncertainty

The variation in the mainstream pressure and coolant flow meter exit pressures contribute to approximately ±2% uncertainty for the mainstream and coolant flow rates. However, the main factor contributing to the uncertainty is the intensity of the PSP recorded by the camera. By using the method of Kline and McClintock [20], the

uncertainty of the film cooling effectiveness at η = 0.1, 0.40 and 0.90 is 15%, 4.5%, and 2%, respectively, for the current study.

5.5 Results and Discussion

5.5.1 Pressure side cutback film effectiveness

To help understand the film effectiveness data, understanding the mainstream and coolant interaction is important. The conceptual view of the mainstream and coolant interaction for the pressure side cutback is shown in Fig. 32. As the coolant exits the cooling hole, vortices are formed near the lip. Similarly, the mainstream air forms a wake region downstream of the slot. Due to the formation of the vortices and the wake, interaction of the coolant with the mainstream is expected. The coolant is also expected to spread in the spanwise and pitch-wise directions.

Film effectiveness data of the PS cutback forms the basis for comparison with new designs. Figure 33 shows the film effectiveness contours for the PS cutback design. The front view (slot and land) is shown in Fig. 33 for MFR 0.30-1.25% and all density ratios while the side walls are shown in Fig. 34 for MFR 0.75-1.25% and all density ratios. The corresponding spanwise film effectiveness and area-averaged data are presented in Fig. 35. The spanwise averaged data is divided into slot only, sidewalls only, land only, slot & land, and slot & land & sidewalls. The spanwise averaged data is taken for the middle 4 slots of the blade with x/s = 0 as the edge of the slot.

In general, the spanwise averaged effectiveness is very high for the PS cutback design. The effectiveness starts from as high as 0.95 for the slot only and slowly decays to around 0.80 at x/s=6 for high MFR. Gao et al. [55] also recorded the same level of

effectiveness for the slot. The lowest MFR (0.30%) has the lowest effectiveness and decays more rapidly. However, the coverage is adequate with the effectiveness approaching 0.5 near the slot exit. Reduced film effectiveness at low MFR is due to lower coolant capacity. As the MFR is increased to 0.5% and above, the effectiveness approaches unity for most of the cases. The effectiveness in general increases with an increase in MFR except for DR=1.0, where the effectiveness increases with MFR varying from 0.30% to 0.5%, then a decrease in effectiveness is witnessed for 0.75-1.00%. The effectiveness again increases with a further increase in MFR. This decrease in effectiveness for MFR= 0.75-1.00% can be attributed to vortex shedding which causes significant mixing of the coolant with the mainstream air. The phenomenon of vortex shedding is not uncommon. Halloway et al. [47, 48], and Choi et al. [52] recorded the negative effect of blowing ratio on film effectiveness and contributed it to vortex shedding in general. Martini et al. [49, 50], and Yan [59] also witnessed that although the film effectiveness increases with an increase in blowing ratio, however, in a certain range of blowing ratios the effectiveness decreases with an increase in blowing ratio. They recorded the effect of vortex shedding in a blowing ratio range of 0.6-0.8 which is similar to the range of blowing ratios in the current study (see Table 7). The data for the sidewalls, as shown in Fig. 34, also shows that the sidewall data is in a similar range of effectiveness as the slots. The sidewall data is slightly lower than the slot and is in the range of 0.8. This is in agreement with the data reported by Gao et al. [55].

The land region, on the other hand, shows a negative effect with an increase in MFR. At higher density ratios, vortex shedding is not witnessed, which is due to lower

coolant momentum resulting in less mixing. The land region shows low effectiveness in the range of 0.15-0.20 for DR=1.0 and 0.25-0.35 for higher density ratios. Gao et al. [55] and Ling et al. [56] reported a similar range of effectiveness for the lands. The combined slot and land effectiveness can be seen to increase from x/s=0 to x/s=6, this is because the land has low effectiveness in the start region, however, due to the tapered angle, the effectiveness increases for the lands which help to increase the overall spanwise averaged effectiveness.

It is interesting to see a strong positive density ratio effect for MFR > 0.30% for the slot, sidewall, and land. For lower MFR the density ratio effective is negative due to insufficient momentum. However, as the MFR is increased, the effectiveness increases by 20-25%. The increase in effectiveness is consistent for a slot, sidewall, and land. With sufficient coolant momentum, better film coverage at higher density ratios is observed. It is also worthy to note that the lands have significantly better film coverage at higher density ratios as compared to lower density ratios. Due to lower, but sufficient momentum, the heavier coolant can spread from the slot to the land region.

Figure 35 also shows the overall area-averaged effectiveness for the slot only, sidewalls only, land only, slot and land, and all combined. It can be seen that the MFR and density ratio effect is positive in general. A clear drop in effectiveness can be seen for MFR=0.75-1.00% for DR=1.0. The “slot only” records the highest area-averaged effectiveness followed by the sidewalls.

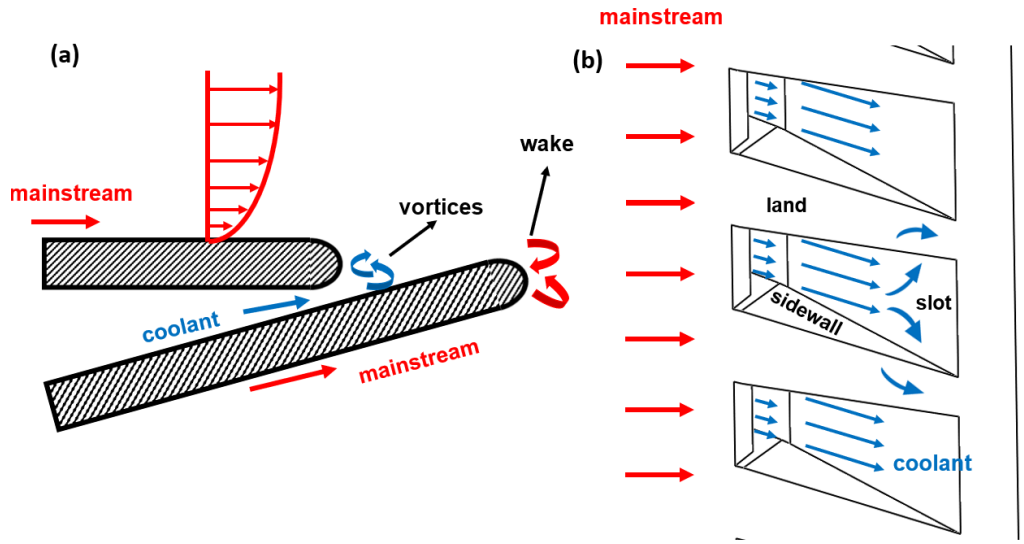

Figure 32. Conceptual view of PS cutback mainstream and coolant interaction

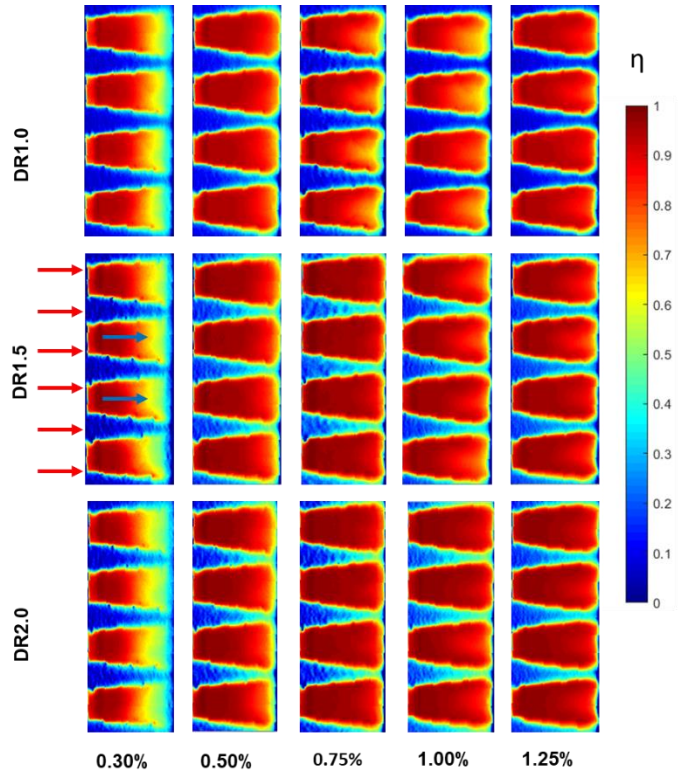

Figure 33. Film effectiveness contours for PS cutback showing slots and lands (arrows in red and blue shows mainstream and coolant direction, respectively)

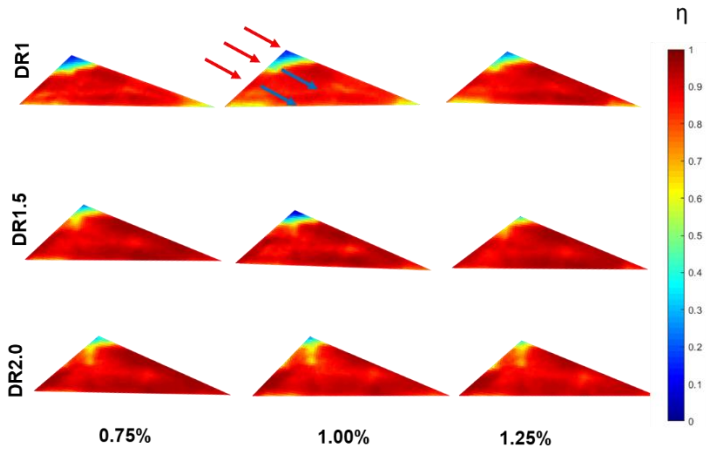

Figure 34. Film effectiveness contours for PS cutback sidewalls (arrows in red and blue shows mainstream and coolant direction, respectively)

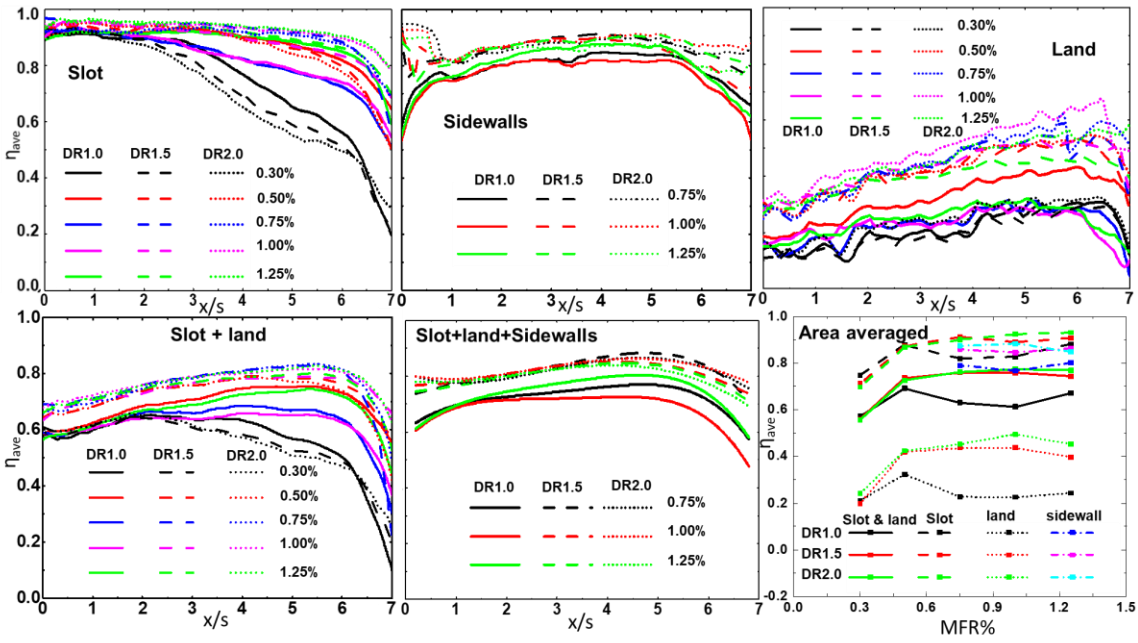

Figure 35. Spanwise averaged effectiveness and area averaged effectiveness for slot, land, sidewalls, and combined

5.5.2 Open Literature comparison

To have confidence with the data of the pressure side cutback design, a comparison is made with the open literature. The slot-only data is compared with the correlation developed by Taslim et al. [46] as well as the experimental data by Gao et al. [55]. Gao's experimental data is in a low-speed wind tunnel; however, the TE design closely resembles the design of the current study except that the land portion in Gao's data is not tapered. The lip thickness for both designs is around 1.0. The present data are also compared with a similar geometry experimentally studied by Ling et al. [56]. Ling's experimental data has both strong tapered and medium tapered lands. The strong tapered configuration has an expansion angle of around 7.5° which is closer to the expansion angle of the present

study (7.16°). However, the blowing ratio studied by Ling et al. is M=1.3 which has been compared to the blowing ratio of M=1.0 in the current study. Parbat et al. [58] carried out a computational study on the same PS cutback and wavy TE design considered in this study. The present study data at MFR=1.25% is compared with Parbat et al. data at MFR=1.50%. The film effectiveness comparison at the closest possible flow conditions is presented in Fig. 36. The comparison shows the current data for the slot is within the range of 10-15% compared to the correlation and the experimental and computational data. The effectiveness comparison for the lands is higher than 20% as compared to Gao et al. data. This is because Gao et al. has no tapered lands while the current design has 7.5° of expansion angle. The data, however, validates the trend for effectiveness data.

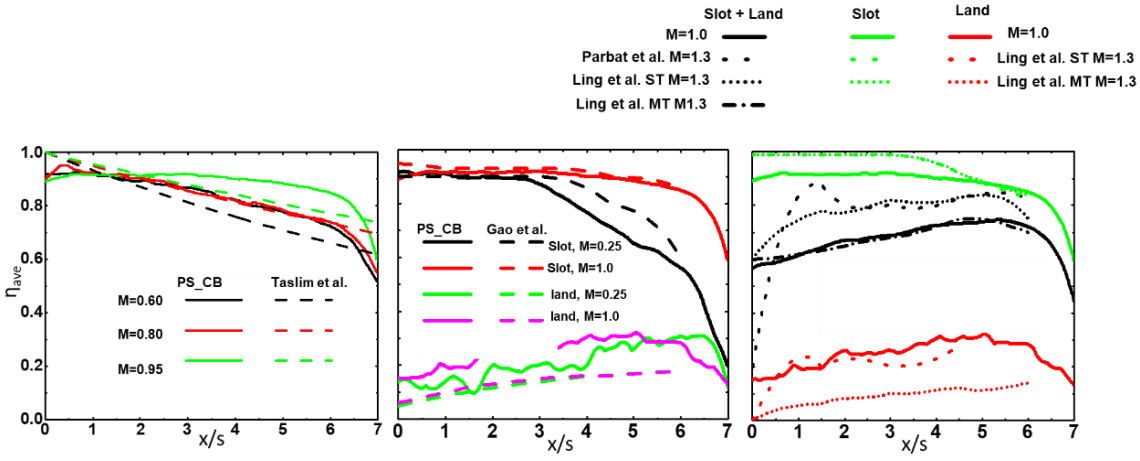

Figure 36. Open literature comparison at DR=1.0

5.5.3 Wavy TE film effectiveness

The conceptual view for the mainstream and coolant interaction for the wavy TE is given in Fig. 37. It can be seen that the coolant is expected to interact with the mainstream and some spreading of coolant to the neighboring holes can take place.

The film effectiveness for the wavy TE for both the pressure and suction surfaces are given in Fig. 38. The spanwise average data for the center four holes is presented in Fig. 39. The magnitude of the film effectiveness exiting the cooling slot is similar to the pressure side cutback slot with the effectiveness as high as 0.95 at the start (x/s=0). However, due to the spanwise average of four holes with only 2 holes on each side of the trailing edge, the spanwise effectiveness for the wavy TE is less than the PS cutback. The spanwise average effectiveness varies in the range of 0.6 to 0.7 for the wavy TE while that for the PS cutback varies in the range of 0.7 to 0.8. At a lower MFR (<0.5%), more coolant is utilized by the suction surface due to a lower mainstream static pressure. For higher MFR values the film effectiveness is approximately the same as that on the PS of the wavy TE design. The comparison between the wavy TE pressure surface and the suction surface can be seen in Fig. 39. Although more coolant may be utilized by the suction surface at higher MFR, both the PS and SS achieve the same level of effectiveness.

A direct comparison between the PS cutback pressure surface and the wavy pressure surface is also presented for all the density ratios in Fig. 40. At lower MFR, due to more coolant utilized by the suction surface for the wavy TE design, a significant difference can be seen between the PS cutback and wavy pressure surface. However, at higher MFR, the wavy pressure surface averaged effectiveness is around 30% lower than

the PS cutback but with almost half of the coolant supply. This certainly is an advantage achieved by the wavy design. The TE with the wavy design can be cooled more as compared to the PS cutback design. Fig. 39 also shows that the density ratio effect is positive similar to the PS cutback design with a 25-30% increase in effectiveness at higher density ratios.

The area-averaged effectiveness gives a more complete picture, as shown in Fig. 41. At a lower MFR, the area-averaged effectiveness is seen to be lower for all the cases. This is due to the insufficient momentum of the coolant to cover the slot. At higher MFR, the area-averaged effectiveness for the PS cutback approaches 0.8 while the wavy is approximately 0.6 at high-density ratios. This is a clear advantage for the wavy TE design. With almost half the coolant on PS and SS surfaces of the wavy design compared to the PS cutback, a still higher spanwise averaged effectiveness of 0.6 is achieved. The density ratio effect is positive with 20-30% effectiveness improvement. The wavy SS effectiveness is higher than the wavy PS effectiveness. This trend agrees with the data reported by Parbat et al. [58], a CFD study on a similar test geometry. They also reported a higher effectiveness for the wavy suction surface as compared to wavy pressure surface for MFR 0.5%-1.0%.

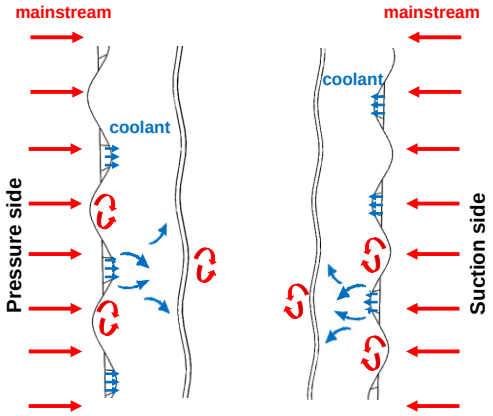

Figure 37. Conceptual view of wavy TE design mainstream and coolant interaction

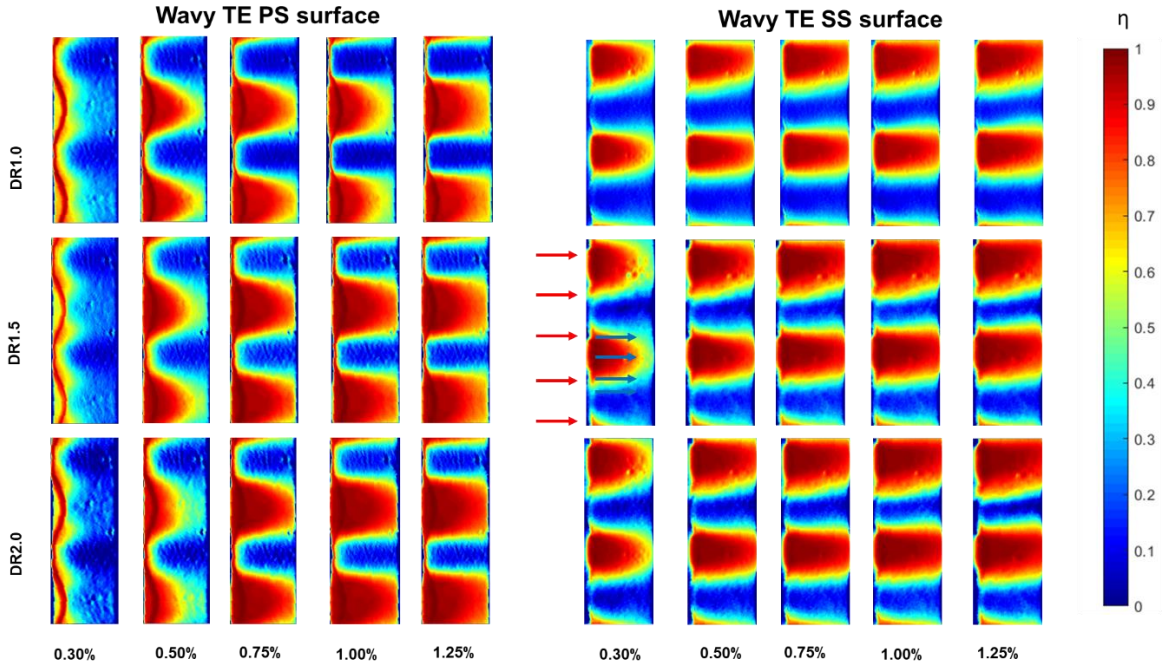

Figure 38. Film effectiveness contours for wavy tailing edge design (arrows in red and blue shows mainstream and coolant direction, respectively)

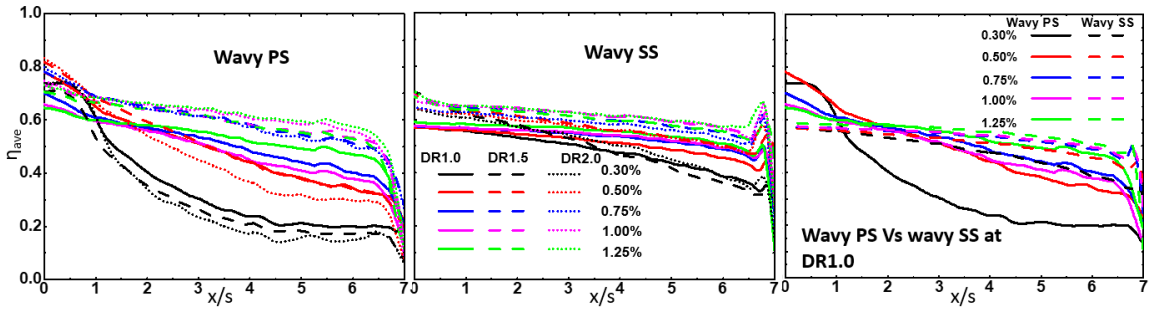

Figure 39. Spanwise averaged film effectiveness for wavy TE

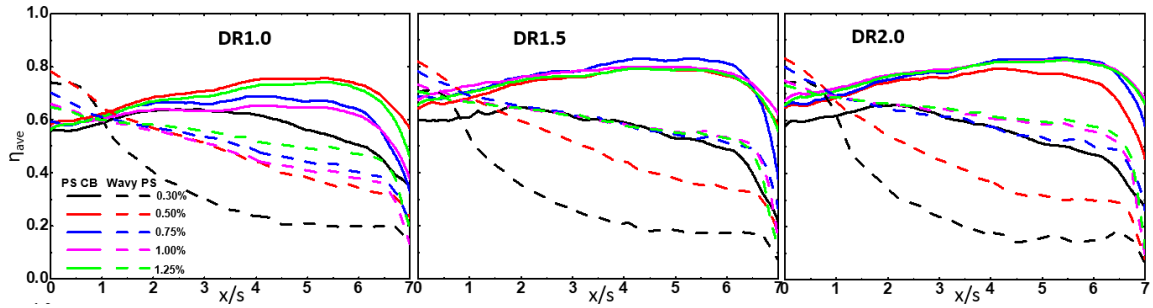

Figure 40. Spanwise averaged film effectiveness for wavy TE vs PS cutback

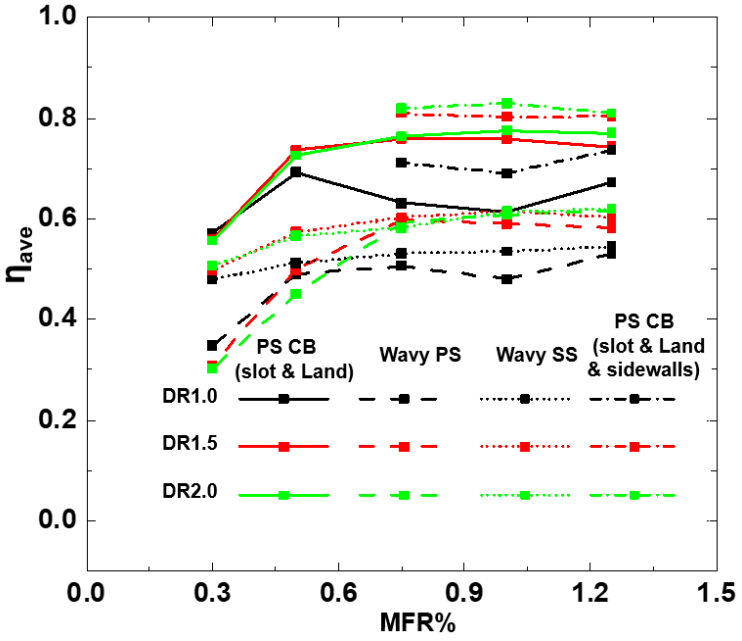

Figure 41. Area averaged film effectiveness comparison for wavy and PS cutback

5.5.4 Aerodynamic Loss

With better overall film effectiveness achieved for the wavy TE, the aerodynamic loss is another aspect that gas turbine designers need. Therefore, the aerodynamic loss ($P_{t,\ exit}/P_{t,\ inlet}$) is measured by traversing an array of 10 pitot-static probes at x/C_{ax} =0.25, downstream of the blade trailing edge as shown in Fig. 42. These 10 pitot-static probes are traversed from the midplane (y/H=0.5) to the top wall (y/H=1.0) with a total of 10 measuring points between the middle and top planes. This gives a total of 100 measuring points to assess the aerodynamic loss, as shown in Fig. 43. The TE of the test blade is at x/L=0 while the PS and SS passages end at x/L=-1 and x/L=1, respectively.

The aerodynamic loss contours at x/C_{ax}=0.25 are presented in Fig. 44 for both the PS cutback and the wavy designs. Both geometries have similar pressure loss results, with the wavy TE showing a slightly increased aerodynamic loss. The MFR effect on the loss is negligible for both designs. Parbat et al. [59] also reported no effect of MFR on aerodynamic loss for a similar range of coolant flow rates for both designs. The reason for the negligible MFR effect could be zero angle of ejection of coolant from the TE. Due to lack of mixing, there is no significant increase in loss as the MFR is varied. It is interesting to see that the aerodynamic loss is highest near the TE suction surface (x/L=0-0.3), this is where the wake region is dominant. This is true for both the PS cutback and the wavy design.

To see if the MFR effect is consistent at different downstream locations, the aerodynamic loss for PS cutback at x/C_{ax} =0.5 is also measured, as shown in Fig. 45. From Fig. 45 it can be seen that the wake region expands and covers x/L=0 to 0.6. The further

the measuring plane from the TE, the larger is the wake region. Increasing the distance from the TE yields a more expanded wake region. The total loss however for the PS cutback at x/C_{ax}=0.5 is lower because of loss recovery. Figure 46 shows a conceptual view of the wake region for x/C_{ax}= 0.25 and 0.5. The wake region is expected to expand with an increase in x/C_{ax}. In addition, the pressure loss measurement at x/C_{ax}=0.5 validates that the MFR effect is negligible. The average aerodynamic loss from the midspan to the top is quantified in Fig. 47. The MFR effect is negligible while the wavy TE shows a slightly higher aerodynamic loss as compared to the pressure side cutback design at x/C_{ax}=0.25.

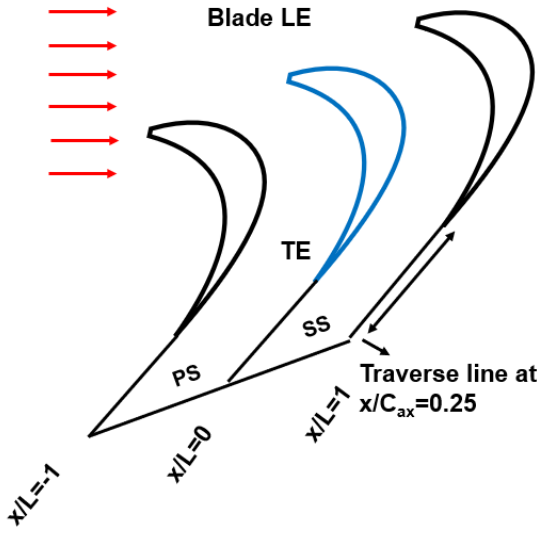

Figure 42. Location of plane for aerodynamic loss measurments

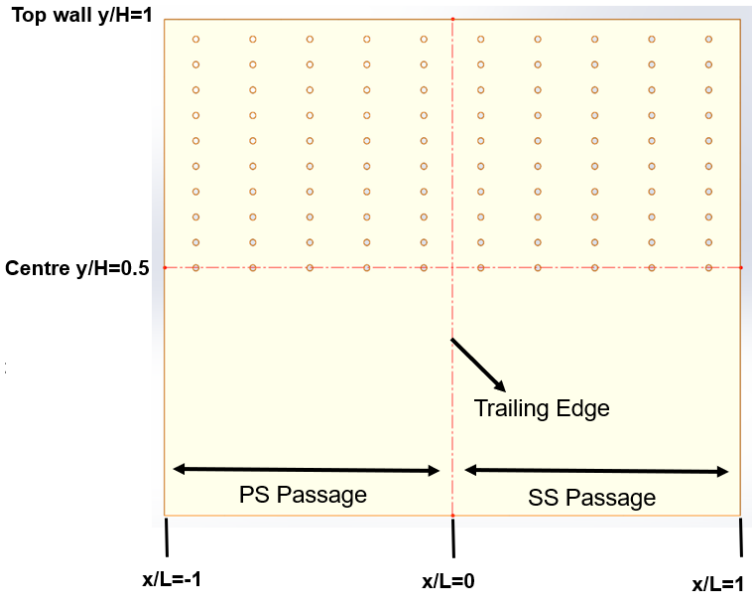

Figure 43. Pitot-static probe locations on the downstream measurement plane

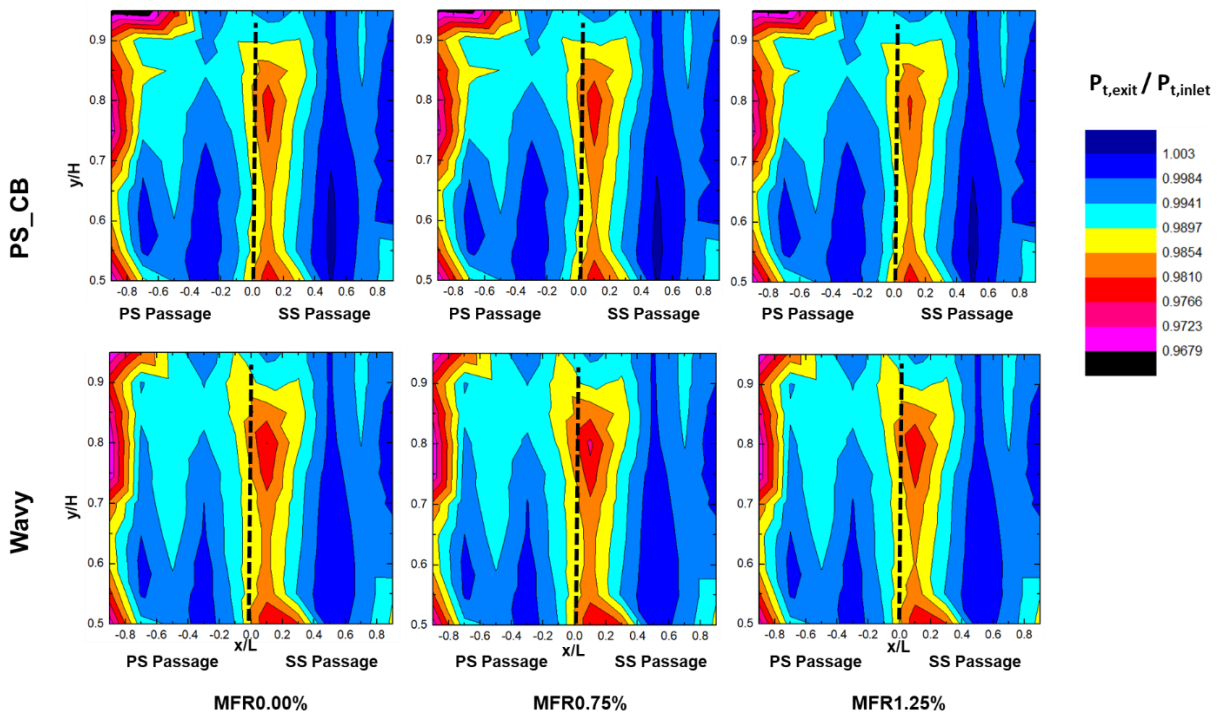

Figure 44. Aerodynamic loss measurement at x/ C_{ax} = 0.25 for wavy and PS cutback

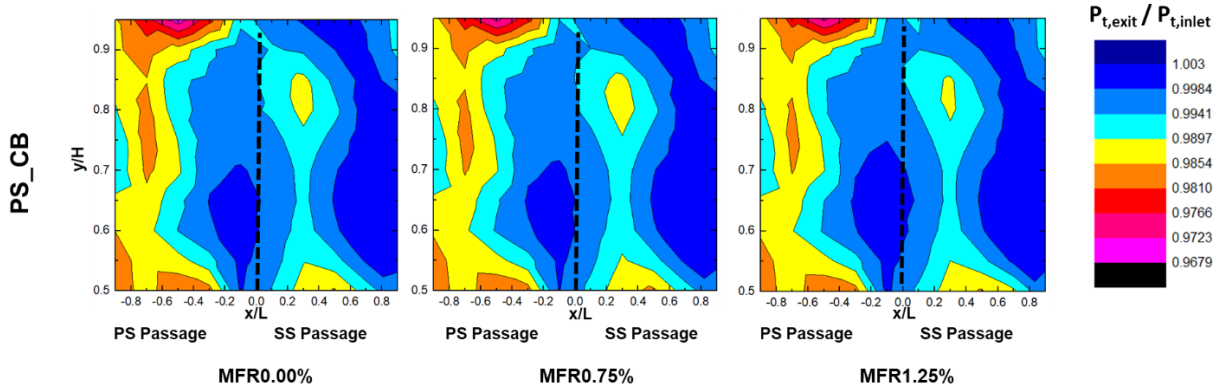

Figure 45. Aerodynamic loss measurement at x/ C_{ax} = 0.50 for PS cutback

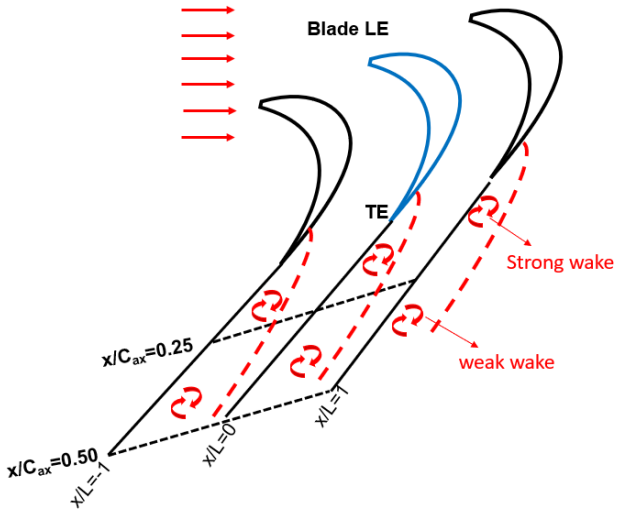

Figure 46. Conceptual view of formation of wake at blade TE

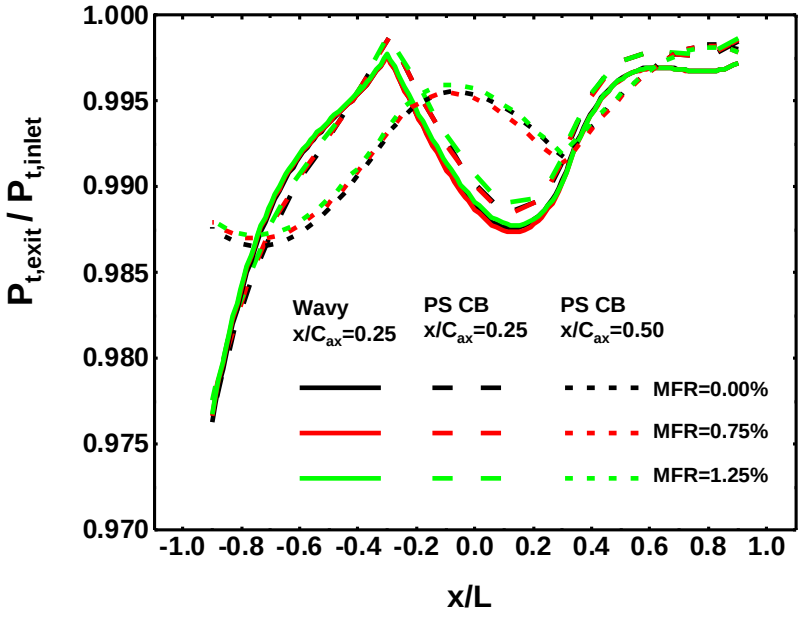

Figure 47. Comparison of laterally averaged pressure ratio for both trailing edge configurations

6. CONCLUSIONS

6.1 Full Scale Turbine Vanes Film Cooling Comparison

Two full-scale turbine vanes were studied and compared under realistic engine flow conditions in a three-vane annular cascade with uncontrolled coolant to the pressure and suction surfaces. The coolant-to-mainstream mass flow ratio (MFR) was varied from 3.12% to 4.61%. Following are the key highlights:

1. The detailed film effectiveness over the entire vane surfaces was captured. Both designs resulted in similar film behavior on the vane surfaces but entirely different coolant split between the pressure and suction surfaces. The coolant distribution through each row of holes was also estimated. The vane 1 design resulted in a more protected pressure surface, with more coolant ejected to the pressure surface as compared to the suction surface. Vane 2 being a similar design to vane 1 but with an additional two rows of holes, offered more protection on the suction surface, with more coolant ejected from this suction surface. Two additional rows of holes redistributed the coolant completely from the pressure surface to the suction surface. A positive MFR impact was witnessed for both the designs with longer traces of film at higher MFR. The MFR impact for the pressure surface was more prominent for vane 1 while vane 2 showed a significant impact of MFR on film effectiveness for both surfaces.
2. This study can help to understand how the film cooling effectiveness changes with introducing new rows of cooling holes at different locations on the vane surface. This

will help the gas turbine designers to better understand the film effectiveness under different cooling configurations. Although the MFR effect is very clear under the range of MFR in this study, a higher MFR range is recommended to study its effect on vane film effectiveness.

6.2 Influence of Coolant Density on Turbine Blade Tip

A flat blade tip design was studied in a 3-blade, linear blowdown cascade under transonic flow conditions to study the parametric effect of coolant blowing ratio, density ratio, and injection designs on the film effectiveness and the over-tip leakage. Different injection scenarios were evaluated by blowing the coolant from tip only as well as both from PS & tip. Following are the key highlights:

1. Over the range of blowing ratios in the current study, a positive effect on the film effectiveness was observed for the blowing ratio in general. The lowest density coolant had less tendency to deflect with the leakage flow due to higher momentum while the heavier density coolant had more tendency to deflect towards the tip surface due to lower momentum. An optimal blowing ratio of M=1.0 was recorded for all density ratios for the given range of blowing ratios. The density ratio effect is the main parameter of interest in the current study. Coolant at higher densities provided wider and more uniform film coverage at the tip. Heavier density coolant (DR=1.5 and DR=2.0) at a higher blowing ratio (M>1.0) provided almost double the film cooling effectiveness as compared to DR=1.0.
2. Leakage flow is also an interesting aspect of this study. The effect of blowing ratio, density ratio, and the injection scenarios on leakage flow was studied. Tip only

injection provided the lowest leakage flow as compared to no coolant blowing cases. A 12 % reduction in over-tip leakage flow was recorded. The effect of density ratio on the leakage flow is insignificant for the range of blowing ratios in this study while the blowing ratio effect is positive.

6.3 Film Cooling and Aerodynamic Loss Measurement of Pressure Side Cutback and Wavy Trailing Edge Design

Two different TE designs were studied in a five-blade linear cascade. Film effectiveness and aerodynamic loss measurements were carried out under steady-state conditions. The coolant-to-mainstream flow was varied from 0.30 to 1.25% while the density ratio was varied from 1.0-2.0. Following are the key highlights:

1. The MFR effect, in general, was recorded to be positive for both designs, especially at the high-density ratios. A reverse trend in effectiveness was recorded for the PS cutback design for MFR=0.75% to 1.00%. This is due to the interaction between the coolant and mainstream, known as vortex shedding. The positive MFR effect is true for the wavy design and the slots of the PS cutback design. The MFR effect on the lands of the PS cutback design is insignificant.
2. The density ratio effect is strongly positive for both designs (wavy and PS cutback). An overall 20-30% increase in effectiveness is witnessed for both designs. The land portion of PS cutback has good coverage of coolant at the high-density ratio due to lower momentum of coolant, thus, providing significant advantage at high-density ratio.

3. Overall, the wavy design proved to be a better design with film cooling on both surfaces. An area averaged effectiveness of 0.6 is achieved at the suction and the pressure surface of the wavy TE design compared to area averaged effectiveness of 0.8 on the pressure surface of the PS cutback design. This shows a clear advantage of the wavy TE with sufficient cooling on both surfaces.
4. The aerodynamic loss for PS cutback and the wavy TE design is in a similar range with a slightly higher loss (1-2%) recorded by the wavy TE.

REFERENCES

[1] Han, J.-C., 2018, "Advanced Cooling in Gas Turbines 2016 Max Jakob Memorial Award Paper," ASME Journal of Heat Transfer, 140(11).

[2] Giller, L., and Schiffer, H.-P., 2012, "Interactions Between the Combustor Swirl and the High-Pressure Stator of a Turbine, " ASME Paper No. GT2012-69157.

[3] Qureshi, I., Smith, A. D., and Povey, T., 2012, "HP Vane Aerodynamics and Heat Transfer in the Presence of Aggressive Inlet Swirl," ASME Journal of Turbomachinery, 135(2).

[4] Lerch, A., Bauer, R., Krueckels, J., and Henze, M., 2020, "Impact of a Combustor–Turbine Interface on Turbine Vane Aerodynamics and Film Cooling," ASME Journal of Turbomachinery, 142(7).

[5] Anthony, R. J., Clark, J. P., Finnegan, J., and Johnson, J. J., 2019, "3D Heat Transfer Assessment of Full-Scale Inlet Vanes With Surface-Optimized Film Cooling: Part 1 — Experimental Results, " ASME Paper No. GT2019-91919.

[6] Shiau, C.-C., Chen, A. F., Han, J.-C., Azad, S., and Lee, C.-P., 2017, "Film Cooling Effectiveness Comparison on Full-Scale Turbine Vane Endwalls Using Pressure-Sensitive Paint Technique," ASME Journal of Turbomachinery, 140(2).

[7] Pedersen, D. R., Eckert, E. R. G., and Goldstein, R. J., 1977, "Film Cooling With Large Density Differences Between the Mainstream and the Secondary Fluid Measured by the Heat-Mass Transfer Analogy," ASME Journal of Heat Transfer, 99(4), pp. 620-627.

[8] Sinha, A. K., Bogard, D. G., and Crawford, M. E., 1991, "Film-Cooling Effectiveness Downstream of a Single Row of Holes With Variable Density Ratio," ASME Journal of Turbomachinery, 113(3), pp. 442-449.

[9] Ekkad, S. V., Han, J. C., and Du, H., 1998, "Detailed Film Cooling Measurements on a Cylindrical Leading Edge Model: Effect of Free-Stream Turbulence and Coolant Density," ASME Journal of Turbomachinery, 120(4), pp. 799-807.

[10] Ethridge , M. I., Cutbirth , J. M., and Bogard, D. G., 2000, "Scaling of Performance for Varying Density Ratio Coolants on an Airfoil With Strong Curvature and Pressure Gradient Effects," ASME Journal of Turbomachinery, 123(2), pp. 231-237.

[11] Gao, Z., Narzary, D. P., Mhetras, S., and Han, J.-C., 2008, "Full-Coverage Film Cooling for a Turbine Blade with Axial-Shaped Holes," AIAA Journal of Thermophysics and Heat Transfer, 22(1), pp. 50-61.

[12] Mhetras, S., Han, J.-C., and Rudolph, R., 2011, "Effect of Flow Parameter Variations on Full Coverage Film-Cooling Effectiveness for a Gas Turbine Blade," ASME Journal of Turbomachinery, 134(1).

[13] Narzary, D. P., Liu, K.-C., Rallabandi, A. P., and Han, J.-C., 2011, "Influence of Coolant Density on Turbine Blade Film-Cooling Using Pressure Sensitive Paint Technique," ASME Journal of Turbomachinery, 134(3).

[14] Dyson, T. E., McClintic, J. W., Bogard, D. G., and Bradshaw, S. D., 2013, "Adiabatic and Overall Effectiveness for` a Fully Cooled Turbine Vane," ASME Paper No. GT2013- 94928.

[15] Wu, J., Zhang, L., Cheng, L.-j., Jiang, R., Fu, Z.-y., and Zhu, H.-r., 2018,"An Experimental Investigation of Full- Coverage Film Cooling Characteristics of a Turbine Guide Vane," ASME Paper No. GT2018-76088.

[16] Yao, C.-y., Zhu, H.-r., Liu, C.-l., Zhang, B.-l., and Li, X.-l., 2020, "Film Cooling and Heat Transfer Performance of a Fully-Cooled Turbine Vane at Varied Density Ratios and Mass Flow Ratios," ASME Paper No. GT2020-15101.

[17] Zhang, S.-q., Liu, C.-l., Guo, Q.-l., Liang, D.-p., and Zhang, F., 2020, "Experimental Study of Full Coverage Film Cooling Effectiveness for a Turbine Blade With Compound Shaped Holes," ASME Paper No. GT2020-15110

[18] Liu, K., Yang, S.-F., and Han, J.-C., 2014, "Influence of Coolant Density on Turbine Blade Film-Cooling With Axial and Compound Shaped Holes," ASME Journal of Heat Transfer, 136(4).

[19] Han, J. C., and Rallabandi, A. P., 2010, "Turbine Blade Film Cooling Using PSP Technique" Front. Heat Mass Transfer, 1(1): 1–2.

[20] Kline, S. J. M. E., 1953, "Describing Uncertainties in Single-Sample Experiments," 75, pp. 3-8.

[21] Han, J. C., Dutta, S., and Ekkad, S., 2012, Gas Turbine Heat Transfer and Cooling Technology, CRC Press, Boca Raton, FL. ISBN:978-1-4398-5568-3.

[22] Ahn , J., Mhetras , S., and Han, J.-C., 2005, "Film-Cooling Effectiveness on a Gas Turbine Blade Tip Using Pressure-Sensitive Paint," ASME Journal of Heat Transfer, 127(5), pp. 521-530.

[23] Kwak, J. S., and Han, J.-C., 2003, "Heat Transfer Coefficients and Film-Cooling Effectiveness on a Gas Turbine Blade Tip," ASME Journal of Heat Transfer, 125(3), pp. 494-502.

[24] Kwak, J. S., and Han, J.-C., 2003, "Heat Transfer Coefficients and Film Cooling Effectiveness on the Squealer Tip of a Gas Turbine Blade," ASME Journal of Turbomachinery, 125(4), pp. 648-657.

[25] Mhetras, S., Narzary, D., Gao, Z., and Han, J.-C., 2008, "Effect of a Cutback Squealer and Cavity Depth on Film-Cooling Effectiveness on a Gas Turbine Blade Tip," ASME Journal of Turbomachinery, 130(2).

[26] Narzary, D., Liu, K., Han, J.-C., Mhetras, S., and Landis, K., 2014, "Turbine Blade Tip Film-Cooling and Heat Transfer Measurements at High Blowing Ratios," ASME Paper No. GT-2014-25793.

[27] Christophel, J. R., Thole, K. A., and Cunha, F. J., 2005, "Cooling the Tip of a Turbine Blade Using Pressure Side Holes—Part I: Adiabatic Effectiveness Measurements," ASME Journal of Turbomachinery, 127(2), pp. 270-277.

[28] Christophel , J. R., Thole, K. A., and Cunha, F. J., 2005, "Cooling the Tip of a Turbine Blade Using Pressure Side Holes—Part II: Heat Transfer Measurements," ASME Journal of Turbomachinery, 127(2), pp. 278-286.

[29] Kim, Y. W., and Metzger, D. E., 1995, "Heat Transfer and Effectiveness on Film Cooled Turbine Blade Tip Models," ASME Journal of Turbomachinery, 117(1), pp. 12-21.

[30] Rezasoltani, M., Lu, K., Schobeiri, M. T., and Han, J.-C., 2015, "A Combined Experimental and Numerical Study of the Turbine Blade Tip Film Cooling Effectiveness Under Rotation Condition," ASME Journal of Turbomachinery, 137(5).

[31] Tamunobere, O., and Acharya, S., 2016, "Turbine Blade Tip Film Cooling With Blade Rotation—Part I: Tip and Pressure Side Coolant Injection," ASME Journal of Turbomachinery, 138(9).

[32] Tamunobere, O., and Acharya, S., 2016, "Turbine Blade Tip Cooling With Blade Rotation—Part II: Shroud Coolant Injection," ASME Journal of Turbomachinery, 138(9).

[33] Azad , G. S., Han , J.-C., Teng, S., and Boyle, R. J., 2000, "Heat Transfer and Pressure Distributions on a Gas Turbine Blade Tip," ASME Journal of Turbomachinery, 122(4), pp. 717-724.

[34] Bindon, J. P., 1989, "The Measurement and Formation of Tip Clearance Loss," ASME Journal of Turbomachinery, 111(3), pp. 257-263.

[35] Moore, J., Moore, J. G., Henry, G. S., and Chaudhry, U., 1989, "Flow and Heat Transfer in Turbine Tip Gaps," ASME Journal of Turbomachinery, 111(3), pp. 301-309.

[36] Key, N. L., and Arts, T., 2004, "Comparison of Turbine Tip Leakage Flow for Flat Tip and Squealer Tip Geometries at High-Speed Conditions," ASME Journal of Turbomachinery, 128(2), pp. 213-220.

[37] Naik, S., Georgakis, C., Hofer, T., and Lengani, D., 2011, "Heat Transfer and Film Cooling of Blade Tips and Endwalls," ASME Journal of Turbomachinery, 134(4).

[38] Pátý, M., Cernat, B. C., De Maesschalck, C., and Lavagnoli, S., 2018, "Experimental and Numerical Investigation of Optimized Blade Tip Shapes—Part II: Tip Flow Analysis and Loss Mechanisms," ASME Journal of Turbomachinery, 141(1).

[39] Arisi, A., Xue, S., Ng, W. F., Moon, H. K., and Zhang, L., 2015, "Numerical Investigation of Aerothermal Characteristics of the Blade Tip and Near-Tip Regions of a Transonic Turbine Blade," ASME Journal of Turbomachinery, 137(9).

[40] Zhang, Q., O'Dowd, D. O., He, L., Wheeler, A. P. S., Ligrani, P. M., and Cheong, B. C. Y., 2011, "Overtip Shock Wave Structure and Its Impact on Turbine Blade Tip Heat Transfer," ASME Journal of Turbomachinery, 133(4).

[41] Shyam, V., Ameri, A., and Chen, J.-P., 2011, "Analysis of Unsteady Tip and Endwall Heat Transfer in a Highly Loaded Transonic Turbine Stage," ASME Journal of Turbomachinery, 134(4).

[42] Jeong, J. Y., Kim, W., Kwak, J. S., and Park, J. S., 2019, "Heat Transfer Coefficient and Film Cooling Effectiveness on the Partial Cavity Tip of a Gas Turbine Blade," ASME Journal of Turbomachinery, 141(7).

[43] Narzary, D., 2010, "Experimental Study of Gas Turbine Blade Film Cooling and Heat Transfer," Ph.D. dissertation, Texas A&M University, CS, TX.

[44] Sivasegaram, S., and Whitelaw, J. H., 1969, "Film Cooling Slots: The Importance of Lip Thickness and Injection Angle," Journal of Mechanical Engineering Science, Vol 11, Issue 1, pp. 22 – 27.

[45] Mukherjee, D. K., 1976, "Film Cooling With Injection Through Slots," ASME Journal of Engineering for Power, 98(4), pp. 556-559.

[46] Taslim, M. E., Spring, S. D., and Mehlman, B. P., 1992, " Experimental investigation of film cooling effectiveness for slots of various exit geometries ". AIAA Journal of Thermophysics and Heat Transfer, Vol. 6 (2), pp302-307.

[47] Holloway, D. S., Leylek, J. H., and Buck, F. A., 2002, “Pressure Side Bleed Film Cooling: Part 1—Steady Framework for Experimental and Computational Results,” ASME Paper No. GT-2002-30471.

[48] Holloway, D. S., Leylek, J. H., and Buck, F. A., 2002, “Pressure Side Bleed Film Cooling: Part 2—Unsteady Framework for Experimental and Computational Results,” ASME Paper No. GT-2002-30472.

[49] Martini, P., Schulz, A., and Bauer, H.-J., 2005, "Film Cooling Effectiveness and Heat Transfer on the Trailing Edge Cutback of Gas Turbine Airfoils With Various Internal Cooling Designs," ASME Journal of Turbomachinery, 128(1), pp. 196-205.

[50] Martini, P., Schulz, A., Bauer, H.-J., and Whitney, C. F., 2005, "Detached Eddy Simulation of Film Cooling Performance on the Trailing Edge Cutback of Gas Turbine Airfoils," ASME Journal of Turbomachinery, 128(2), pp. 292-299.

[51] Cunha, F. J., and Chyu, M. K., 2006, “Trailing-Edge Cooling for Gas Turbines,” AIAA Journal of Propulsion and Power, Vol. 22, No. 2, pp. 286-300.

[52] Choi, J.-h., Mhetras, S., Han, J.-C., Lau, S. C., and Rudolph, R., 2008, "Film Cooling and Heat Transfer on Two Cutback Trailing Edge Models With Internal Perforated Blockages," ASME Journal of Heat Transfer, 130(1).

[53] Krueckels, J., Gritsch, M., and Schnieder, M., 2009, “Design Considerations and Validation of Trailing Edge Pressure Side Bleed Cooling,” ASME Paper No. GT-2009-59161.

[54] Horbach, T., Schulz, A., and Bauer, H.-J., 2011, "Trailing Edge Film Cooling of Gas Turbine Airfoils—External Cooling Performance of Various Internal Pin Fin Configurations," ASME Journal of Turbomachinery, 133(4).

[55] Gao Z., Rhee, D-H., and Han, J. C., 2013, “Turbine Blade Trailing Edge Slot Film Cooling Using PSP Technique” International Journal of Transport Phenomena, Vol. 13, pp 193-205.

[56] Ling, J., Elkins, C. J., and Eaton, J. K., 2015, "The Effect of Land Taper Angle on Trailing Edge Slot Film Cooling," ASME Journal of Turbomachinery, 137(7).

[57] Wong, T. H., Ireland, P. T., and Self, K. P., 2016, "Film Cooling Effectiveness Measurements on Trailing Edge Cutback Surface and Lands Following Novel Cross Corrugated Slot Geometry." ASME. Paper No. GT-2016-57371.

[58] Parbat, S., Yang, L., Chyu, M., Siw, S. C., and Lee, C.-P., 2019, "Numerical Study of Heat Transfer in Novel Wavy Trailing Edge Design for Gas Turbine Airfoils." ASME Paper No. GT-2019-91123.

[59] Yan, X, 2020,"Very Large Eddy Simulation of Film Cooling Effectiveness on Trailing Edge Cutback." ASME. Paper No. GT-2020-15780.

[60] Uzol , O., Camci, C., and Glezer, B., 2000, "Aerodynamic Loss Characteristics of a Turbine Blade With Trailing Edge Coolant Ejection: Part 1—Effect of Cut-Back Length,

Spanwise Rib Spacing, Free-Stream Reynolds Number, and Chordwise Rib Length on Discharge Coefficients," ASME Journal of Turbomachinery, 123(2), pp. 238-248.

[61] Uzol , O., and Camci, C., 2000, "Aerodynamic Loss Characteristics of a Turbine Blade With Trailing Edge Coolant Ejection: Part 2—External Aerodynamics, Total Pressure Losses, and Predictions," ASME Journal of Turbomachinery, 123(2), pp. 249-257.

[62] Chen, A. F., Shiau, C.-C., and Han, J.-C., 2017, "Turbine Blade Platform Film Cooling With Fan-Shaped Holes Under Simulated Swirl Purge Flow and Slashface Leakage Conditions," ASME Journal of Turbomachinery, 140(1).

[63] Gao, Z., Narzary, D., and Han, J.-C., 2009, "Turbine Blade Platform Film Cooling With Typical Stator-Rotor Purge Flow and Discrete-Hole Film Cooling," ASME Journal of Turbomachinery, 131(4).